Journal of Water Process Engineering 93 (2026) 110868

Contents lists available at ScienceDirect

Journal of Water Process Engineering

journal homepage: www.elsevier.com/locate/jwpe

Adsorption kinetics and solution chemistry governing organophosphorus herbicide removal from water by magnetic ion exchange resin

Martyna Krajewska, Phuong B. Trinh, Andrea I. Schäfer *

Institute for Advanced Membrane Technology (IAMT), Karlsruhe Institute of Technology (KIT), Hermann-von-Helmholtz-Platz 1, 76344 Eggenstein-Leopoldshafen, Germany

ARTICLE INFO

Editor: Mingmei Ding

Keywords:
Physico-chemical water treatment
Adsorption
Micropollutants
Glyphosate (GLY)
Aminomethylphosphonic acid (AMPA)

ABSTRACT

Glyphosate (GLY) and its main metabolite, aminomethylphosphonic acid (AMPA), are highly polar, anionic micropollutants frequently detected in surface and groundwater, posing threats to the environment and human health. This study investigates the removal of GLY and AMPA by a commercially available magnetic ion exchange resin (MIEX) and explains how adsorption kinetics and solution chemistry govern the process under environmentally relevant conditions. MIEX is compared with polymer-based spherical activated carbon (PBSAC), a high-capacity adsorbent with a fundamentally different removal mechanism. Batch experiments under varying MIEX doses, initial contaminant concentrations, pH, and ionic strengths provided insights into the removal of GLY and AMPA. A MIEX dose of 10 mL/L achieved removal of 91 ± 3% for GLY and 79 ± 5% for AMPA from an initial concentration of 1 μg/L. Although PBSAC exhibited higher equilibrium adsorption capacities, MIEX provided rapid uptake through readily accessible ion-exchange sites. Adsorption saturation was not approached within the investigated concentration range, and the adsorption isotherm showed near-linear behavior, indicating that adsorption capacity was not the limiting factor. Adsorption performance depended strongly on pH and ionic strength, with the highest removal at pH 4–10. Increasing ionic strength markedly reduced adsorption kinetics, particularly for GLY, supporting an electrostatically-controlled and reversible ion-exchange mechanism. The results demonstrate that, under environmentally relevant conditions, the performance of MIEX toward GLY and AMPA is governed more strongly by adsorption kinetics, solution chemistry, and the accessibility of ion-exchange sites than by equilibrium adsorption capacity and highlight the importance of kinetic considerations for short-contact water treatment.

1. Introduction

1.1. Water contamination by glyphosate

Glyphosate (GLY) was first synthesized in 1950. In 1974, U.S. Environmental Protection Agency (EPA) permitted the use of GLY in the USA under the trade name Roundup, developed by Monsanto (USA), while European regulatory approval was granted in 2002 [1]. Since its introduction, GLY has been extensively used worldwide, raising major concerns about the potential environmental, animal, and human health implications. Numerous studies (in vitro, in animals, and even in humans) have reported divergent and sometimes contradictory findings regarding its toxicity [1,2]. A notable breakthrough in the ongoing debate was the retraction, in late 2025, of a widely cited study evaluating the human health risks of GLY exposure, which had previously concluded no significant carcinogenic, reproductive, or endocrine risks associated with GLY or Roundup [3]. The article was withdrawn by the journal due to concerns regarding academic integrity and the credibility of the reported findings [4]. Contamination of water by GLY and its main metabolite, aminomethylphosphonic acid (AMPA) is predominantly linked to agricultural runoff [5]. However, municipal wastewater discharges and household phosphonate use have also been identified as significant sources of GLY and AMPA in aquatic environment [6]. GLY and AMPA are detected worldwide at a broad concentration range (0.2 to 370 μg/L) in groundwater and surface water [7,8]. In Europe, reported concentrations reach up to 57 μg/L, while typical concentrations detected in Germany are 1.35 μg/L of AMPA and 0.55 μg/L for GLY [6].

The EU Drinking Water Directive sets a parametric value of 0.1 μg/L for individual pesticides, including GLY and AMPA, and 0.5 μg/L for the total concentration of all pesticides and relevant metabolites in drinking water [9]. Ongoing concerns over the environmental persistence and

* Corresponding author.
E-mail address: Andrea.Iris.Schaefer@kit.edu (A.I. Schäfer).

https://doi.org/10.1016/j.jwpe.2026.110868
Received 23 June 2026; Received in revised form 27 August 2026; Accepted 29 August 2026
Available online 12 September 2026

List of abbreviations

AC	activated carbon
AMPA	aminomethylphosphonic acid
AOP	advanced oxidation process
DOC	dissolved organic carbon
EPA	Environmental Protection Agency
EU	European Union
GLY	glyphosate, N-(phosphonomethyl)glycine
IX	ion exchange
LOD	limit of detection
MIEX®	magnetic ion exchange resin
NF	nanofiltration
NOM	natural organic matter
PBSAC	polymer-based spherical activated carbon
PFAS	*per*- and polyfluoroalkyl substances
UV	ultraviolet

potential health risks associated with GLY remain. In the absence of a qualified majority agreement among EU Member States, the European Commission renewed the approval of GLY as an active substance in plant protection products within the European Union under stricter conditions, until 2033 [10,11]. This makes the issue of removing herbicides from water even more important, although preventing the entry of such contaminants into waterways would be a more cost-effective strategy.

Despite increasing efforts to remove GLY and AMPA from water, important questions remain regarding the applicability of different treatment technologies. The following sections provide the necessary context by reviewing GLY and AMPA properties, available removal technologies, the principles of ion exchange, and the applications and interactions of magnetic ion exchange resins with GLY and AMPA.

1.2. GLY and AMPA properties

The GLY molecule is small, with a hydrodynamic diameter of 0.62 nm [12] and a molecular weight of 169 g/mol [13–16], while AMPA is even smaller. GLY contains strongly polar functional groups (amine, carboxyl, and phosphonate moieties), which enable hydrogen bonding and ionic interactions. Thus, GLY is highly polar and strongly hydrophilic, which has implications for challenging removal from water and demanding analytical detection.

Both GLY and AMPA have ionizable functional groups, which undergo stepwise deprotonation depending on pH. Under environmentally relevant pH of 6–8, the carboxyl and phosphonate groups of GLY are largely deprotonated, while the amine group remains protonated, resulting in a net negative charge [17] (Fig. 7). The pH-dependent speciation of GLY and AMPA is illustrated in Fig. 6, and the chemical properties are listed in Table 1.

1.3. Methods for GLY and AMPA removal

In soils, GLY degradation is driven by microorganisms through C–N bond cleavage, forming AMPA and glyoxylate, or through C–P bond cleavage to sarcosine and inorganic phosphate (a pathway considered to be of limited environmental relevance) [21]. AMPA requires the C–P lyase enzyme for further degradation [21] and is generally more persistent in the environment than GLY [6]. Since other GLY metabolites degrade faster than AMPA, the AMPA pathway appears to be predominant [21]. Abiotic degradation of GLY can occur via hydrolysis, photolysis (ultraviolet radiation), and chemolysis (peroxide and mineral oxidation) [22,23]; however, these processes are generally slower than biodegradation [22]. Under abiotic conditions, GLY degradation may occur through cleavage of either the C–N bond (yielding AMPA), the C–P bond, or simultaneously, depending on the reaction environment and conditions. The former pathway may be kinetically and thermodynamically favored [23].

Table 1
Chemical properties of GLY and AMPA.

	GLY N-(phosphonomethyl) glycine		AMPA aminomethylphosphonic acid	
Molecular formula	$C_3H_8NO_5P$		CH_6NO_3P	
Structural formula	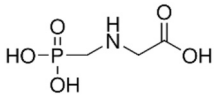		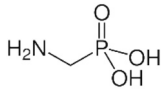	
Molecular weight, g/mol	169.07	[13–16]	111.04	[13]
Solubility in water at 25 °C, g/L	12	[13,15,18]	50	[13]
pK_a values	0.8, 2.6, 5.6, 10.6	[13,16]	1.8, 5.4, 10.2	[13]
Density, g/mL	0.5	[16,19]	ND	
Polarity	high	[13]	high	[13]
H-donors/acceptors	4/6	[13]	3/4	[13]
Hydrodynamic diameter, nm	0.62	[12]	0.49	[12]
Log K_{ow}	−2.9 to −4.1	[13,16]	- 2.2	[13]
Dipole moment, D	7.5 9.7	[14] [19]	ND	
pH (1% solution in water)	2.5	[16,19]	ND	
Max level in EU, µg/L	0.1	[20]	0.1	[20]

ND - no data available.

Multiple treatment technologies in conventional water treatment can reduce the load of GLY and AMPA, but removal differs markedly [24] and is often insufficient to reach the EU guideline value for individual pesticides (0.1 µg/L) [20]. Coagulation, acting as a pretreatment step in drinking water preparation, may contribute to the removal of GLY and AMPA via complexation with coagulants and adsorption/co-precipitation. However, efficiency strongly depends on coagulant type and dose, as well as raw water properties such as pH, natural organic matter (NOM) composition, particle concentration, and hardness [24,25]. Slow sand filtration can provide partial removal of GLY/AMPA through adsorption and biodegradation, while its performance is influenced by operational conditions, time since last cleaning, and temperature [25]. Chlorination can remove GLY and AMPA [26] at concentrations and times typical for water treatment facilities [25]. Ozonation, as part of the disinfection stage of water treatment, is reported to be highly effective for GLY and AMPA degradation, but depends on the ozone concentration and pH [24,25]. Chemical and photodegradation [27–29], as well as advanced oxidation processes (AOPs) [30], have been investigated for the removal of GLY; however, toxic by-products can be generated [16,25]. Membrane technology, particularly nanofiltration (NF), is a promising chemical-free technique [31]. NF removes 70–80% of GLY and AMPA from a 50 µg/L solution at 25 bar [31], which is energy-consuming and generates a concentrate that require further treatment.

Adsorption is a relatively low-cost, low-footprint, chemical-free technology. It is a well-established technology, simple operation, no transformation by-product formation with possible adsorbent regeneration [32]. Activated carbon (AC) is available in various forms, such as granular AC [25], industrial residues [33], biochar [34], resins [35], and modified AC [36]. Removal of 60–80% of GLY from an original concentration of 30 µg/L has been reported [25]. Polymer-based spherical AC (PBSAC) combines high surface area (1600–2100 m^2/g) with high pore volume (0.6–1.3 cm^3/g), uniform spherical shape, and controlled characteristics (pore size distribution) [37]. Energy-intensive regeneration, slow adsorption kinetics, and lower selectivity reduce its applicability [38].

Although AC is widely applied for micropollutant (MPs) removal from water, its performance toward small, hydrophilic, and charged compounds is often limited and may be further compromised by organic matter competing for sorption sites and blocking the microporous structure. As GLY is a typical example of such challenging micropollutants, in theory, highly efficient removal by PBSAC would not be expected. Nevertheless, 0.5 g/L PBSAC achieved >95% GLY removal from the initial concentration of 1 μg/L. [13] As discussed in the following section, ion exchange (IX) resins have been proposed as an alternative to AC [38], particularly for charged GLY and AMPA.

1.4. Principles and functioning of ion-exchange resins

IX resins are cross-linked polymeric materials functionalized with fixed charged groups that enable reversible ion exchange in aqueous solution [39]. A brief overview of ion-exchange resin classification is provided in Section 1.1 of the Supporting Information. Strong-base anion exchangers, such as MIEX (magnetic ion exchange resin) with quaternary ammonium groups, remain fully ionized over a wide pH range and therefore effectively interact with negatively charged species [39,40]. The IX properties of materials arise from the electrostatic interactions between fixed charged groups on the polymeric matrix and mobile counter-ions. When a resin is in contact with an aqueous medium, the resin counter-ions become mobile and can be reversibly exchanged with ions of the same charge from the surrounding medium. Simultaneously, co-ions of the same charge as the resin are partially excluded due to electrostatic repulsion. This phenomenon is known as the Donnan exclusion [41]. At high ionic strength, the Donnan potential is reduced (due to charge screening), and thus selectivity decreases. The IX process is competitive and reversible, and depends on the solution pH, ionic strength, and the affinity of the ionized solute compared to the background ions [42]. IX resins are considered for micropollutants removal due to their ability to selectively capture charged species through electrostatic interactions and secondary interactions with polymer matrix (hydrogen bonding, van der Waals, polar, and π-π interactions) [43]. In aqueous environments, the resin swells upon water uptake, increasing the internal pore accessibility and exposing internal IX sites [44]. This structural expansion facilitates interactions with hydrated ions (like GLY^- and $AMPA^-$), enhancing their removal.

1.5. MIEX application in water treatment

MIEX® (Magnetic Ion EXchange resin) was developed as a commercial product for NOM removal in water treatment to avoid the formation of disinfection by-products [45,46]. As a strong anion-exchange resin, MIEX contains fixed covalently bound quaternary ammonium groups (with trimethylamine groups), which provide the permanent positive charge over a wide pH range [44].

MIEX features much smaller beads (180–250 μm [44]) than conventional IX resins such as Dowex 21 K XLT (300–1200 μm) [47] and Amberlite IRA 400 (300–800 μm) [48], resulting in a higher surface area (approx. 21.5 m^2/g [44,49,50]) and faster adsorption kinetics compared to traditional anion exchange resins [51]. Unlike conventional IX resins, MIEX contains a magnetic component (iron oxide) within its polymeric structure [52]. This magnetic component allows the beads to agglomerate and settle easily, improving their separation from treated water [46]. In water treatment, MIEX is typically applied in a slurry contactor configuration, where resin beads are mixed with water. Continuous mixing reduces the thickness of the boundary layer and enhances external mass transfer. As a result, film diffusion limitations are significantly less pronounced than those in conventional fixed-bed configurations. In large-scale applications, MIEX is operated in completely mixed reactors or fluidized systems (such as dual-stage reactor, high-rate reactor, fluidized IX, suspended IX reactor with mechanical mixing, or a hydraulic labyrinth mixing) [53,54], as a continuous-flow process. In such systems, the majority of the resin is continuously recycled, while a portion is periodically withdrawn for regeneration [46]. Following contact, the resin is efficiently separated through magnetically enhanced settling and returned to the contactor [46,55]. In full-scale systems, MIEX is typically operated with hydraulic retention times of 10–30 min, in specific cases extended to 45–60 min [44,46]. The efficiency of NOM removal is governed by the resin dose and saturation, which are regulated through the balance between the stream of regenerated resin supplied to the reactor and the stream of saturated resin withdrawn from the reactor [53]. Typical MIEX doses in water treatment vary from 5-10 mL/L [56] to 5–20 mL/L [57]. However, the required dose and contact time depend on the quality of the water matrix and target contaminants [56]. Regeneration of saturated MIEX is achieved via simple ion-exchange process using NaCl brine, in which sorbed anions are exchanged for chloride ions at the quaternary ammonium sites [49]. The NaCl concentration commonly used for regeneration is 10–15% (*w*/w) [58], corresponding to approximately 1.8–2.8 M (1800–2800 mM) NaCl.

Previous studies have shown that MIEX preferentially removes low- and medium-molecular-weight organic compounds, particularly in the range of 0.5–1.5 kDa [51], while exhibiting limited effectiveness toward high and very high-molecular-weight (>50 kDa) and colloidal dissolved organic matter of microbial origin due to size exclusion within the pores [59]. Gao et al. investigated the removal of perfluoroalkyl and polyfluoroalkyl substances (PFAS) using MIEX Gold, which exhibited high removal (90% from an initial concentration of 1500 μg/L) for hydrophobic PFAS [60]. All the above suggest that small, negatively charged molecules such as GLY and AMPA are especially well suited for removal by MIEX due to their rapid diffusion and efficient access to IX sites. However, the applicability of MIEX for GLY and AMPA removal and its performance relative to PBSAC have not yet been systematically evaluated. Therefore, the present study compares both adsorbents under environmentally relevant conditions.

1.6. GLY/AMPA interactions with magnetic ion exchange resins

Several interactions are anticipated between GLY/AMPA and MIEX, depending on the distance between solute and resin surface or functional groups (Fig. 1), including electrostatic interaction, ion exchange, hydrogen bonding, van der Waals interactions, and interactions with iron oxide. GLY/AMPA is attracted to the resin via electrostatic interactions, while retention is primarily governed by ion exchange between phosphonate and carboxyl groups and quaternary ammonium sites (with trimethylamine groups). Electrostatic attraction occurs mainly in the pH > 5.6, where GLY and AMPA carry a net negative charge and coexist with the permanently positively charged MIEX. This interaction can act over relatively long distances (~10 nm under very low ionic strength and ~ 3 nm at 10 mM NaCl as the basic conditions used in this study), depending on the Debye length [61]. Its magnitude is

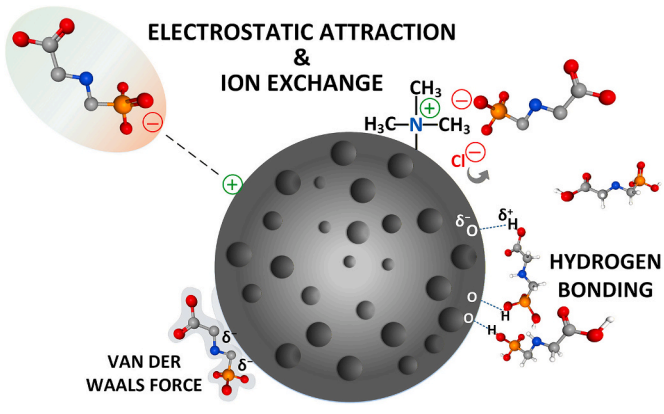

Fig. 1. Possible interactions of GLY with MIEX.

governed by the charge and charge density of both the surface and the adsorbate, as well as the solution ionic strength. Ion exchange is triggered when GLY and AMPA approach the quaternary ammonium sites (N^+), resulting in the release of Cl^-. Ion exchange between the quaternary ammonium group and GLY/AMPA dominates under conditions where the solutes are ionized, and the resin is in the functional pH range. At neutral pH, the phosphonate group of GLY/AMPA is the most reactive toward ion exchange with MIEX due to the stronger negative charge and predominant deprotonation, followed by the carboxyl group. Under neutral conditions, the amino group remains protonated and positively charged, not contributing to anion exchange. Hydrogen bonding (at very short distances <1 nm) may occur between the amino group –NH, carbonyl group –C=O or hydroxyl group –OH on MIEX [62] and hydroxyl group –OH, amino group $–NH_2$ or phosphonate group $-PO_3^{2-}$ on GLY. However, because the polymer matrix of MIEX is relatively less hydrophilic compared to GLY/AMPA, hydrogen bonding formation may be limited to the hydration shell surrounding GLY/AMPA, whose structure is pH-dependent. Van der Waals forces (at very short distances <1 nm) may occur between the methyl group $–CH_3$, carbonyl group –C=O, or aromatic rings on the polymethacrylate–divinylbenzene matrix of MIEX [62] and methylene groups $-CH_2-$ of GLY. No π stacking can take place since there is no aromatic ring in the GLY molecule [63].

The primary role of iron oxide incorporated in the polymer matrix of MIEX is to facilitate the separation of the resin from the solution after the resin loading [46]. Interactions of GLY/AMPA with the magnetic iron oxide component (maghemite γ-Fe_2O_3) [44] may occur, but such interactions are expected to be insignificant. MIEX is a macroporous IX resin with a bead size of 180–250 μm, with iron oxide particles dispersed within the polymer matrix [45,62]. Even though the magnetic component constitutes 20–25% *w*/w of the MIEX bead [64], the interaction between the magnetic components and GLY is expected to occur only near the bead surface or pore openings and therefore involve only a limited accessible surface area. Consequently, any direct interaction between GLY and the magnetic component is considered to be minimal compared to ion exchange by the quaternary ammonium sites. Santos et al. [65] suggest an affinity between ferric compound (α-γ-Fe_2O_3) and the phosphonic group of GLY. According to Park et al. [66], the basic mechanism of GLY removal from water by the magnetic component (in that case, it was Fe_3O_4 nanoparticles with a significantly larger surface area) is the covalent coupling of organic molecules onto inorganic oxide surfaces. The formation of metal–oxygen–phosphorus (M–O–P) bonds proceeds rapidly at ambient temperature [66]. Identification and characterization of interactions governing the adsorption are fundamental for optimizing the operating conditions of the separation process [67].

Beyond dominant electrostatic interaction via quaternary ammonium group and complementary physical adsorption, the MIEX matrix further facilitates GLY removal [68]. The hydrophilic polyacrylate backbone promotes interactions with strongly hydrophilic GLY, enhancing diffusion into the resin beads and rapid access to the IX sites [69]. Moreover, the small hydrodynamic diameter of GLY (0.62 nm) allows the penetration into the macroporous structure (pore size of tens of nanometers), facilitating access to functional groups. These properties make MIEX a promising material for GLY removal.

Although PBSAC can effectively remove GLY and AMPA from water [13], its performance is limited by slow intraparticle diffusion within its porous structure. In contrast, MIEX provides readily accessible IX sites and operates via a fundamentally different uptake mechanism. The following research questions are addressed in this study: (i) How does the adsorption by MIEX compare with that of PBSAC, a high-capacity adsorbent with fundamentally different working characteristics? (ii) How do adsorption kinetics and accessibility of ion-exchange sites govern the removal of GLY and AMPA by MIEX? (iii) To what extent do operational conditions and solution chemistry control the adsorption on MIEX? The novelty of this study lies in demonstrating that under environmentally relevant conditions, the performance of MIEX toward GLY and AMPA is governed more strongly by kinetic accessibility of IX sites and solution chemistry than by equilibrium adsorption capacity itself.

2. Materials and methods

2.1. Structure, properties, and performance of MIEX compared with PBSAC

MIEX bead matrix is made of moderately cross-linked macroporous methacrylate [46], while the main functional groups on the resin surface are positive quaternary ammonium [64]. MIEX beads create a slurry of quaternized copolymer mixture (60–100%) in water (<40%) [70,71]. MIEX® DOC and Gold were provided by IXOM WATERCARE, USA.

Table 2 lists the properties of both resins and provides a comparison with the selected AC adsorbent, PBSAC, provided by Blücher, Germany. MIEX Gold has the same bead dimensions and total IX capacity as MIEX DOC, but a larger surface area and a rougher surface, as shown by scanning electron microscopy micrographs [44,52,78], resulting in greater spacing between exchange groups and better accessibility of functional groups with less steric hindrance from organic molecules [79]. The batch uniformity of MIEX is presented in **Figs. S1** and **S2**.

The specific physical form of MIEX requires storage and operation as a suspension to maintain the product quality. Consequently, unlike AC materials, the MIEX dose is conventionally expressed in volumetric units rather than as dry mass. Although determination of the dry mass is possible under controlled laboratory conditions, it is impractical in technological applications [44]. The dried MIEX mass was determined to be 250 mg/mL (details of the calculations are provided in SI) [44]. Therefore, MIEX doses are reported in volumetric units throughout this study, while the corresponding dry mass equivalents are provided to facilitate comparison with PBSAC and are shown in **Table S9**.

2.2. Chemicals and solution chemistry

The background electrolyte was prepared as a mixture of 5 mM $NaHCO_3$ (dissolved from powder of 99.7% purity, VWR, Germany) and 50 mM NaCl (dissolved from powder of 99.5% purity, Thermo Fisher

Table 2
Selected properties of MIEX® DOC and Gold compared with PBSAC properties.

	MIEX resins® (DOC/Gold)		PBSAC 200 μm	
Appearance	Brown opaque beads, porous and smooth surface	[45]	Black, uniform, spherical particles	
Form	90% (*v*/v) slurry in water[a]		Dry granules	
Application range	pH 3–10[a]		Tested in 2–12	[13]
BET surface area, m^2/g	21.47	[44,49,50,72]	1436	[13]
Magnetic content	20–25% (*w*/w)	[64]	N/A	
Mean particle size, μm	150–180 180–250[a]	[45,62]	200	[73]
Main functional group	Quaternary ammonium	[64,74]	Oxygen-containing groups 5%	
IX capacity, meq/mL	DOC: 0.4–0.5 DOC: 0.52 Gold: 0.4–0.55	[64,75] [76] [64,75]	N/A	
Average pore size, nm	5.87 27.48	[50] [62]	1.3	[73]
Polymer	Macroporous poly methacrylate/ divinyl benzene	[75]	Polymer carbonized in manufacturing	
Surface charge	Positive in pH 3–11, decreasing above pH 6	[52,77]	Insignificant net surface charge	[13]

N/A – not applicable.
[a] provided by manufacturer.

Scientific, USA) in Milli-Q water. For each experiment, the background solution was diluted to obtain a concentration of 1 mM $NaHCO_3$ and 10 mM NaCl. Powders of GLY (98%) and AMPA (99%) were from Sigma-Aldrich, USA. A mixed stock solution containing both herbicides was prepared by dissolving GLY and AMPA powder in Milli-Q water at a concentration of 100 mg/L of each compound (primary stock solution). The primary stock solution was diluted with Milli-Q water to obtain a solution of 100 μg/L, which was further used with background electrolyte to prepare the desired concentration of GLY and AMPA in the feed solution. In most experiments, the feed solution contained 1 μg/L GLY and 1 μg/L AMPA. In other cases, the specific values were given. The feed solution had a conductivity of approximately 1400 μS/cm and a pH of 8.1 ± 0.1, unless otherwise indicated. The chemical properties of GLY and AMPA are listed in Table 1. The GLY and AMPA speciation was described previously [13] and is presented in the background of Fig. 6. To evaluate the performance of MIEX at varying pH (pH 2, 4, 6, 8, 10, 11, and 12), the stock solution was adjusted to the desired pH levels using different volumes of 1 M HCl (prepared from 37% HCl solution from Roth, Germany) or 1 M NaOH (prepared by dissolving the NaOH pellets (purity ≥99%) from Merck, Germany). For experiments at various ionic strengths, an appropriate volume of 100 g/L NaCl (purity 99.5%, Thermo Fisher Scientific, USA) was added to 1 mM $NaHCO_3$ to obtain 1, 2, 5, 10, 15, and 20 g/L NaCl solutions.

2.3. GLY and AMPA static adsorption on MIEX compared with PBSAC

Although MIEX is typically operated in continuous resin contact and recirculation with regeneration of a fraction of the resin [44,46], batch experiments are used to determine equilibrium time, adsorption capacity, and kinetics under controlled conditions, providing insights for scale-up [54]. Static adsorption experiments were conducted in batch mode by contacting resin with MP-containing water. The method is illustrated in **Fig. S3**. The kinetics of GLY and AMPA removal by MIEX DOC (batch 16–3572) and Gold (batch 16-2562D) were determined, uptake by adsorption quantified, and equilibrium evaluated. Before the experiment, fresh MIEX resin beads were rinsed ten times with MilliQ water to remove the residual manufacturing solution [45]. The resin was allowed to settle for 5 min in a 5 mL or 12 mL syringe (depending on the targeted dose), and the desired volumes of suspension were measured. Varying MIEX volumes corresponding to the desired concentrations (0.5–25 mL/L) of solid material were further transferred into conical flasks already containing GLY and AMPA.

Due to the magnetic properties of the adsorbent, a magnet was used to accelerate the settling. After dosing MIEX, the incubator shaker Innova 43R (New Brunswick, USA) was set to keep a constant temperature of 20 °C at a shaking speed of 260 rpm for 26 h of the experiment. MIEX-free supernatant samples (1.5 mL) were collected using a pipette (100–1000 μL, Eppendorf, Germany) at specific intervals (0, 2, 5, 10, 15, 30, 45 min, and 1, 3, 5, 7, 9, 24, and 26 h), stored in brown glass vials, and refrigerated at 4 °C until analyzed. The adsorption performance of MIEX and PBSAC toward GLY and AMPA was evaluated under identical batch conditions, following the same sampling scheme and analysis. The methodology for static adsorption experiments with PBSAC (used here for performance comparison) was analogous and was described previously [13]. Both adsorbents were tested at the same dosage of 0.5 g/L (equivalent to 2 mL/L for MIEX; Fig. 3) and at their respective critical doses of 2.5 g/L (10 mL/L) for MIEX and 1 g/L for PBSAC (**Fig. S6**), corresponding to the lowest doses beyond which removal no longer increased substantially. The removal and specific mass adsorbed were calculated for both materials, and data were fitted to pseudo-first-order and pseudo-second-order models to compare adsorption kinetics. The film mass transfer coefficient (k_f) and surface diffusion coefficient (D_s) were estimated for GLY and AMPA adsorbed by MIEX and PBSAC at a 0.5 g/L dose (equivalent to 2 mL/L for MIEX), following the methodology presented previously [80], and are presented in **Table S6**. The maximum adsorbed mass monolayer on PBSAC and the maximum IX capacity for MIEX were further calculated (**Table S7**).

2.4. Analytical methods

The pH and conductivity were measured using a Universal Multi-Parameter Portable pH/Cond 3320 (WTW, Germany). GLY and AMPA concentrations were quantified by liquid chromatography with tandem mass spectrometry (LC-MS/MS) manufactured by PerkinElmer, USA, comprising an ultra-high-performance liquid chromatograph (LX50) with a Q-Sight 420 triple-quadrupole mass spectrometer. A non-derivatization-stage method was used to measure GLY/AMPA concentration in water, reducing analytical errors [13]. The limit of detection (LOD) for LC-MS/MS analysis was determined at 10 ng/L. The detailed methodology is described in a previous study [13] and **Table S1**. The calibration is shown in **Fig. S4.**

2.5. Calculations and data analysis

The adsorption parameters, kinetic models with assumptions, and adsorption isotherm models used are listed in **Table S2**. Equations used to calculate electrolyte-dependent parameters (ionic strength and Debye length) are presented in **Table S3**. The error analysis is provided in **Table S4**. Results of five independent experiments are presented in **Fig. S5** for experimental repeatability. The experimental data were fitted using OriginPro 2024 software (Origin Lab Corporation, USA). Pseudo-first and pseudo-second-order kinetics models were applied to analyze the interactions between adsorbate (GLY/AMPA) and adsorbent (MIEX) and fit to Henry, Langmuir, and Freundlich adsorption models.

3. Results and discussion

3.1. MIEX performance for GLY and AMPA removal

To verify whether MIEX is capable of removing GLY and AMPA from the solution, initial experiments were conducted using MIEX DOC and MIEX Gold resins at a dose of 10 mL/L under environmentally relevant GLY/AMPA concentration of 1 μg/L (Fig. 2).

Both MIEX DOC and Gold demonstrated substantial removal of GLY and AMPA from the solution. The removal values for AMPA were 79 ± 5% and 62 ± 7% for MIEX DOC and Gold, respectively, while the corresponding values for GLY were 91 ± 3% and 80 ± 4%. Removal of both GLY and AMPA increased rapidly during the first 2 h of contact with the adsorption steady-state reached within 4 h for GLY and AMPA on MIEX DOC and Gold. Removal of AMPA was consistently lower than that of GLY (**Fig. S14**). However, for AMPA, MIEX DOC performs 17% better than MIEX Gold. As the structure of the resin matrix and the spatial distribution of functional groups may affect adsorption and ion exchange kinetics [81], the structural differences between MIEX DOC and Gold may also influence the adsorption of small molecules such as GLY and AMPA. As GLY and AMPA are small (hydrodynamic diameter of 0.62 and 0.49 nm, respectively), the steric hindrance is much smaller than NOM (of heterogeneous size fractions from humics of ~1 kDa (and diameter < 2 nm) to biopolymers with molecular weight of >10 kDa [82]). Since MIEX DOC offers higher local charge density and electrostatic potential, it may enhance the adsorption of micropollutant molecules, and thus higher removal is expected.

As presented in Fig. 2, AMPA interacts more efficiently with closely packed ion-exchange sites of MIEX DOC. In contrast, for larger molecules (such as NOM), the higher surface area of MIEX Gold is advantageous, as it appears to reduce steric hindrance and improve adsorption [44,78]. Superior removal by MIEX DOC compared to Gold has also been reported for small emerging organic contaminants with molecular weights <300 g/mol, including simazine, bisphenol A, and carbamazepine [79].

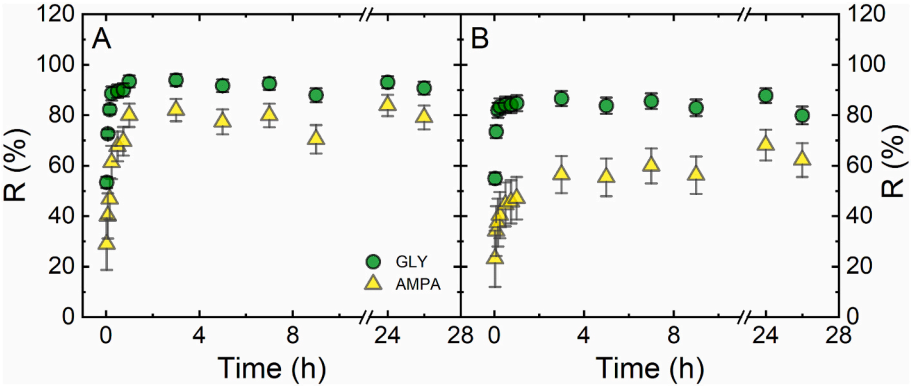

Fig. 2. GLY and AMPA removal (R, %) by MIEX DOC (A) and MIEX Gold (B) in time (MIEX dose 10 mL/L, initial GLY and AMPA concentration 1 μg/L, 1 mM $NaHCO_3$, 10 mM NaCl, 20 °C, 260 rpm, pH 8.1 ± 0.1). (For interpretation of the references to colour in this figure legend, the reader is referred to the web version of this article.)

3.2. Comparison of PBSAC and MIEX for removal of GLY and AMPA

To assess the adsorption behavior of MIEX, its performance was examined in relation to a high-capacity PBSAC [13], under identical experimental conditions at equal dose of 0.5 g/L, which is 2 mL/L of MIEX (Fig. 3). Because PBSAC and MIEX rely on fundamentally different mechanisms, their comparison provides insight into the relative importance of adsorption capacity and the accessibility of adsorption sites. At the same applied dose, both MIEX DOC and PBSAC effectively removed GLY and AMPA, although PBSAC achieved higher adsorbed masses. Specifically, MIEX removed 70 ± 5% of GLY and 22 ± 11% of AMPA, while PBSAC achieved removal of 95 ± 10% and 55 ± 15% for GLY and AMPA, respectively. For MIEX, the concentration of both analytes reached a plateau rapidly, indicating that adsorption likely

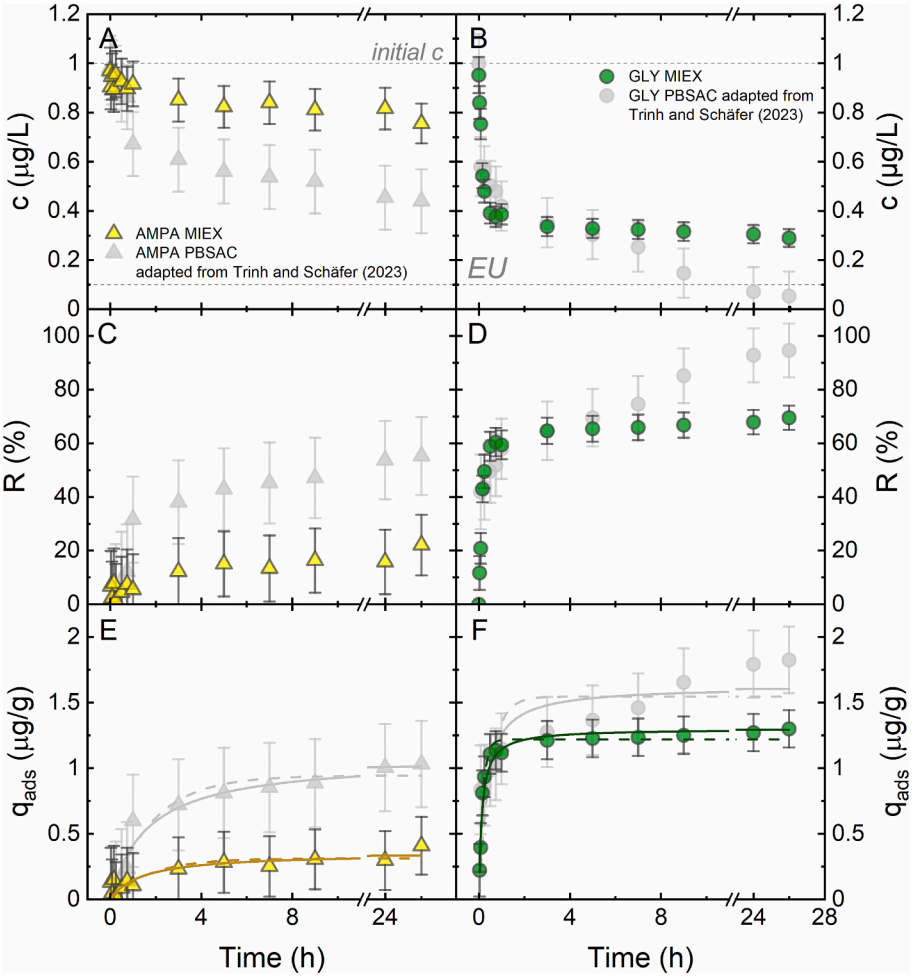

Fig. 3. Comparison of AMPA and GLY (A-B) concentration (c, μg/L), (C-D) removal (R, %), and (E-F) specific mass adsorbed (q_{ads}, μg/g) by PBSAC 200 μm adapted from Trinh and Schäfer (2023) [13] and MIEX DOC in time (adsorbent doses 0.5 g/L, initial GLY and AMPA concentration 1 μg/L, 1 mM $NaHCO_3$, 10 mM NaCl, 20 °C, 260 rpm, pH 8.1 ± 0.1). Dashed and solid curves in the bottom row are the best fits according to the first and second-order kinetic models, respectively.

occurred predominantly at readily accessible exchange sites, which is characteristic of ion-exchange interactions. For PBSAC, the equilibrium was not reached within this contact time, which can be attributed to the intraparticle diffusion within the porous structure of AC, which needs more time to reach equilibrium. Thus, direct comparison of equilibrium parameters alone does not fully express their adsorption behavior and fitting the kinetic models were conducted [83]. Both pseudo-first and pseudo-second-order models mathematically fit the adsorption data of GLY and AMPA on MIEX (**Table S5**).

However, the pseudo-first model is more physically reasonable and better represents the mechanism for GLY and AMPA adsorption on MIEX. The pseudo-first-order model assumes that the adsorption rate is proportional to the number of unoccupied sorption sites [83], which is consistent with the electrostatic interactions and ion exchange governing GLY/AMPA removal on MIEX. In this system, adsorption is primarily governed by mass transfer, specifically the transport of adsorbate to the MIEX surface. In contrast, the pseudo-second-order model is often interpreted as surface-reaction-controlled or chemisorption-type adsorption [83], which is less consistent with the predominantly electrostatic ion-exchange interactions expected for these anionic compounds on MIEX. The second-order kinetic model was previously reported to better characterize the adsorption of GLY and AMPA on PBSAC [13]. Although MIEX exhibited lower equilibrium adsorbed mass than PBSAC (**Table S5**), it showed a higher apparent first-order rate constant for GLY adsorption (5.57 ± 0.39 1/h to 2.04 ± 0.63 1/h for PBSAC), indicating a more rapid approach to steady state. For GLY, PBSAC showed a slightly higher adsorbed mass at equilibrium (q_e=1.62 ± 0.09 μg/g, based on pseudo-second-order fitting) compared to MIEX (q_e=1.22 ± 0.02 μg/g, based on pseudo-first order fitting). For AMPA, PBSAC exhibited approximately three times higher q_e than MIEX (q_e=1.08 ± 0.06 vs. 0.31 ± 0.03 μg/g, respectively), while both adsorbents showed comparable apparent adsorption rates. High equilibrium capacities reduce adsorbent demand, but adsorption kinetics and the accessibility of adsorption sites may become equally important under short-contact operating.

The rapid uptake of GLY by MIEX is consistent with the initial adsorption at readily accessible IX sites with limited diffusion constraints. This is reflected by the higher initial adsorption rate (r_0) and film mass transfer coefficient (k_f) of MIEX compared with PBSAC (**Table S6** and section **4.1** of SI), indicating faster mass transfer during the early stages of adsorption [80]. In contrast, slightly higher surface diffusion coefficients (D_s) for PBSAC suggest more effective adsorbate migration within porous structure after the initial adsorption step. Together with the much higher internal surface area of PBSAC, this is consistent with continued adsorption during the later stages of the process. Thus, PBSAC continues to accumulate adsorbate over time, leading to higher equilibrium capacities, whereas MIEX benefits from rapid uptake at readily accessible sites. Despite its lower theoretical adsorption capacity, MIEX exhibited considerably higher utilization of the available adsorption sites under the tested conditions (**Table S7**), suggesting that readily accessible IX sites are used more efficiently than the extensive internal porosity of PBSAC.

Although PBSAC 200 μm exhibits a BET (Brunauer–Emmett–Teller) surface area approximately 70 times higher than that of MIEX DOC (1436 m^2/g [13] and 21.5 m^2/g [44,49,50,72], respectively), the sizes of the adsorbent beads are comparable (200 μm for PBSAC and 180 μm for MIEX). Therefore, the difference in surface area arises predominantly from the large internal porosity of PBSAC. This indicates that a large number of the adsorption sites in PBSAC are located within micropores, which may not be fully accessible to GLY and AMPA due to diffusion limitations and steric constraints. In contrast, MIEX provides fewer but more readily accessible IX sites. To investigate how these differences translate into practical operation, both adsorbents were evaluated at their critical doses (10 mL/L equal to 2.5 g/L of MIEX and 1 g/L of PBSAC), defined as the lowest adsorbent doses beyond which no substantial increase in removal is observed (**Fig. S6).** Under these conditions, after 26 h, MIEX achieved slightly higher AMPA removal (80 ± 5%) than PBSAC (62 ± 10%). Notably, adsorption on PBSAC was still progressing after 26 h, indicating that equilibrium had not yet been reached. These observations demonstrate that equilibrium adsorption capacity alone does not fully determine practical performance and highlight the importance of adsorption site accessibility and contact time.

3.3. Enhancement of GLY and AMPA removal at varying MIEX dose

In the magnetic anion exchange processes, the resin dose and contact time are the primary parameters whose relationship has been utilized in reactor design [44]. The experiments with varying MIEX doses were conducted for both MIEX types, and the results are presented in Fig. 4. The experimental parameters (pH and conductivity) and GLY/AMPA concentration over time are presented in **Table S8** and **Fig. S7**.

With increasing MIEX dose, corresponding to a larger amount of readily accessible ion-exchange sites, GLY and AMPA removal improved up to 10 mL/L, reaching 91 ± 3%. Further increasing the dose above 10 mL/L resulted in only marginal improvements in removal. Even at 25 mL/L, removal increased only to 94 ± 2% by approx. 3%. For MIEX Gold, the removal increased from 77 ± 4% for GLY and 42 ± 9% for AMPA at a dose of 5 mL/L to 94 ± 2% for GLY and 89 ± 4% for AMPA at 25 mL/L. The GLY removal is 20% higher than AMPA for doses up to 5 mL/L, and the difference decreases in higher adsorbent doses, being equal at 25 mL/L.

Theoretical calculations (**Table S9**) revealed that the number of available IX sites substantially exceeded the number of GLY and AMPA molecules even at the lowest resin doses. Therefore, the limited removal observed at low doses (0.5–1 mL/L) cannot be attributed to exhaustion of IX sites. Moreover, the apparent first-order rate constants (k_1), which describe the rate at which adsorption approaches equilibrium, increased markedly with increasing resin dose (**Table S10**), consistent with improved accessibility of exchange sites at higher resin doses. This effect was most pronounced up to 15 mL/L, beyond which no consistent increase in the k_1 was noted and only marginal improvements in removal were observed. These observations suggest that adsorption performance at environmentally relevant concentrations is governed primarily by kinetic accessibility rather than by the total number of exchange sites.

The critical MIEX dose of 10 mL/L, was used for further experiments. This value falls within the amount of MIEX resin typically used in water treatment [56,57]. The hydraulic retention time in full-scale reactors typically ranges from 10 to 60 min [44,46]. Batch experiments with magnetic IX resins usually last approximately 60 min [44]. For GLY, the steady-state adsorption reached after 2 h suggests that MIEX performance in practical applications occurs under kinetically influenced rather than adsorption equilibrium.

3.4. MIEX effectiveness at elevated initial GLY and AMPA concentrations

To evaluate whether adsorption capacity may limit MIEX performance, GLY and AMPA removal was investigated over a wide range of initial GLY and AMPA concentrations (0.1–1000 μg/L). The results for MIEX DOC and Gold are shown in Fig. 5. The experimental parameters (pH and conductivity) and the GLY and AMPA concentrations over time are presented in **Table S11** and **Fig. S8**.

The performance of MIEX depends on the concentrations of GLY and AMPA in solution. Removal of GLY remained close to 90% in the entire concentration range tested. However, removal of AMPA at both resin types decreases significantly with initial herbicide concentration, reaching only 20% and 10% for MIEX DOC and Gold, respectively, at 1000 μg/L. Guideline values for GLY were reached only when the initial concentration was ≤1 μg/L.

Stoichiometrically, there are 350 times more IX sites than micropollutant molecules at 1000 μg/L of GLY and AMPA, suggesting that

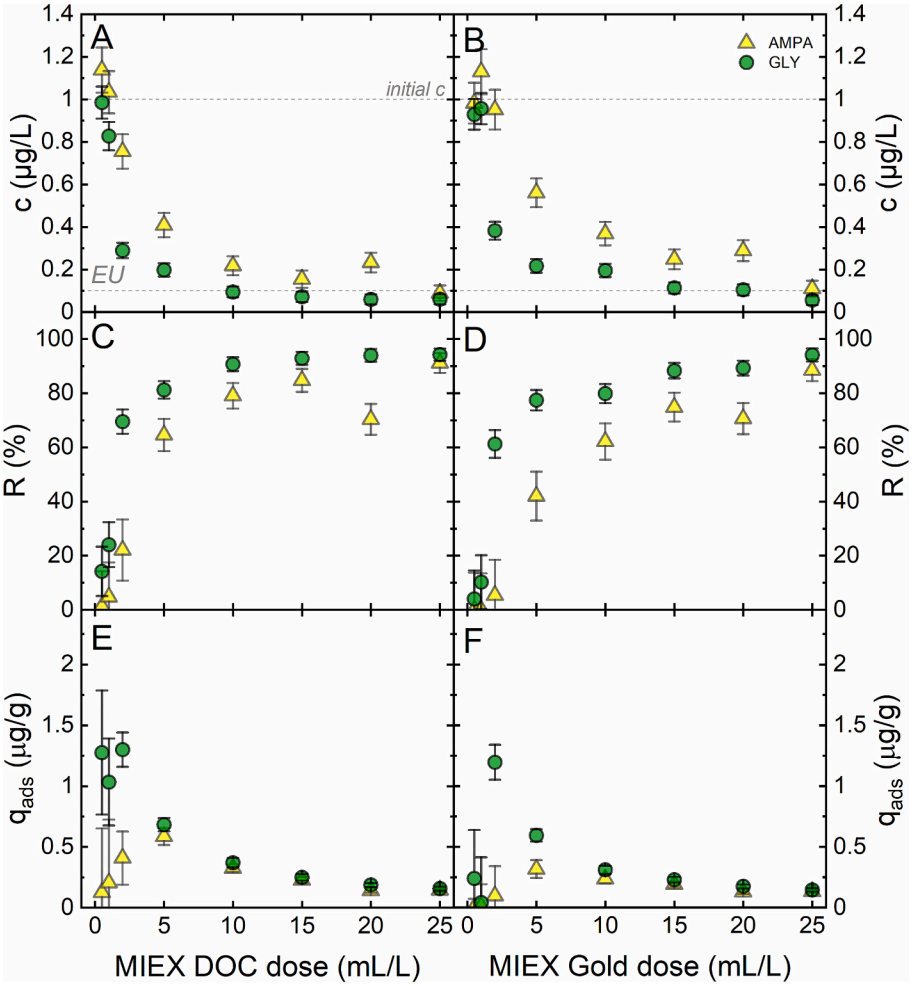

Fig. 4. GLY and AMPA (A-B) concentration (c, µg/L), (C-D) removal (R, %), and (E-F) specific mass adsorbed (q_{ads}, µg/g) as a function of MIEX DOC and MIEX Gold dose after 26 h of exposure (initial GLY and AMPA concentration 1 µg/L, 1 mM $NaHCO_3$, 10 mM NaCl, 20 °C, 260 rpm, pH 8.1 ± 0.1). (For interpretation of the references to colour in this figure legend, the reader is referred to the web version of this article.)

exhaustion of the overall adsorption capacity is unlikely to limit GLY/AMPA removal by MIEX. Adsorption isotherms (**Fig. S9** and **Table S12)** revealed distinct concentration-dependent adsorption behavior for GLY and AMPA. GLY showed a near-linear concentration dependence, with a Freundlich exponent close to unity ($1/n_F$ = 0.95 ± 0.02), indicating near-Henry behavior over the investigated concentration range. The linear Henry model represents the limiting case in which adsorption is proportional to solute concentration, typically associated with low adsorbate coverage [84]. The Freundlich model, an empirical equation without a strict mechanistic interpretation, is commonly associated with adsorption on heterogeneous surfaces and may also describe multilayer adsorption [85]. When the Freundlich exponent is close to or equal to 1, the equation reduces to the linear Henry isotherm and implies early-stage adsorption. Therefore, the Freundlich fit is used here as an empirical description of concentration-dependent uptake and is not interpreted as evidence of multilayer adsorption. In contrast, even when it is not evident in the log-scale graph, the adsorbed mass AMPA increased toward a maximum; this adsorption pattern is evident as the removal decreased from 90 to 20% with increasing initial concentration from 1 to 1000 µg/L. This 'decay' pattern was better described by the Langmuir model, indicating a stronger tendency toward site-limited uptake. The Langmuir model yielded a finite apparent maximum adsorption capacity for AMPA of 133 ± 12 µg/g. This model assumes monolayer adsorption and no interactions between adsorbate molecules [85], making it conceptually well suited to describing ion-exchange processes [40]. These observations, together with the large stoichiometric excess of IX sites and the very low utilization of the theoretical ion-exchange capacity, indicate that even at concentrations several orders of magnitude above environmentally relevant levels, MIEX operates far below its theoretical capacity for GLY and AMPA. Therefore, MIEX performance under practical conditions is more likely to be influenced by adsorption kinetics, solution chemistry, and the accessibility of effective IX sites rather than on exhaustion of the overall ion-exchange capacity.

3.5. *Role of pH in GLY and AMPA removal by MIEX*

To investigate the ability of MIEX to remove GLY and AMPA across pH outside the typical range of natural waters, adsorption experiments were conducted at pH from 2 to 12. The results are presented in Fig. 6 and **Fig. S10**, and the corresponding experimental parameters (pH and conductivity) are provided in **Table S13**.

The MIEX effectiveness at various pH generally depends on the combined effects of: changes in GLY/AMPA speciation and MIEX surface charge, increased competition from hydroxide ions for ion-exchange sites, and enhanced molecular hydration that weakens electrostatic interactions. At the acidic pH of 2, GLY removal is low since the net molecular charge of GLY approaches 0 under these conditions, which reduces electrostatic interactions and hampers the ion exchange (Fig. 7). The ion exchange may be partially inhibited by the excess chloride ions

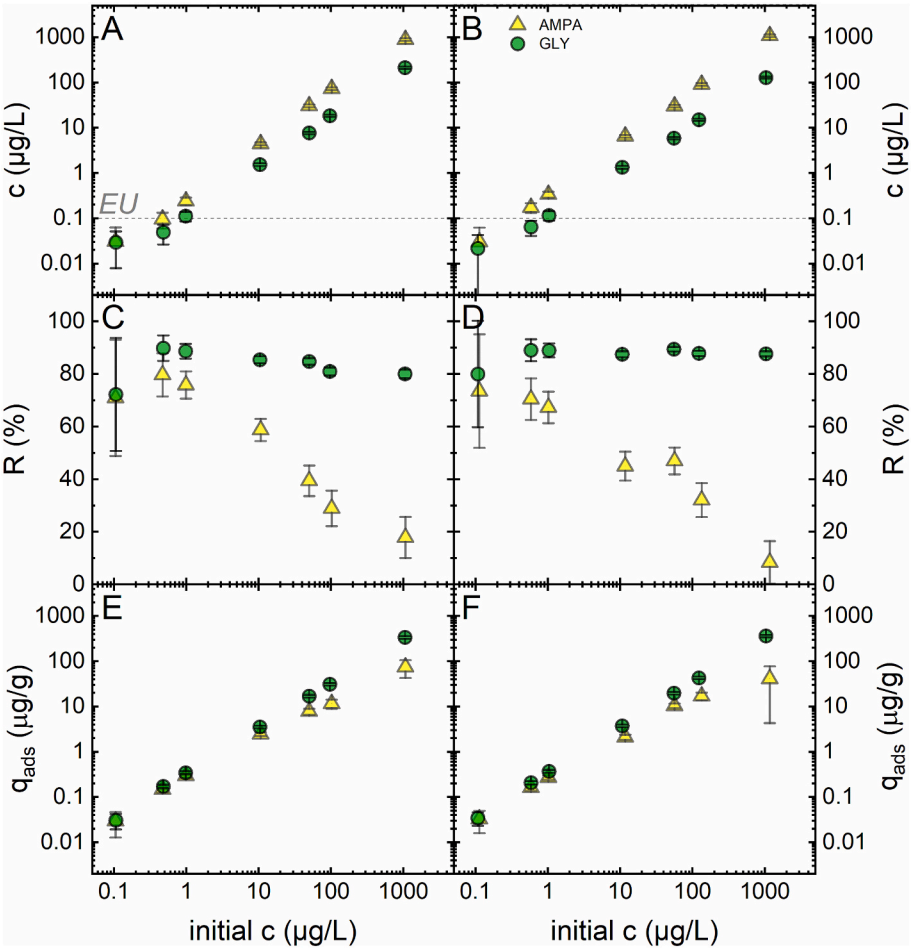

Fig. 5. GLY and AMPA (A-B) concentration (c, µg/L), (C-D) removal (R, %), and (E-F) specific mass adsorbed (q_{ads}, µg/g) by MIEX DOC (A) and MIEX Gold (B) at various GLY and AMPA initial concentration (MIEX dose 10 mL/L, 1 mM $NaHCO_3$, 10 mM NaCl, 20 °C, 260 rpm, pH 8.1 ± 0.1). (For interpretation of the references to colour in this figure legend, the reader is referred to the web version of this article.)

originating from pH adjustment with HCl [86] (the ionic strength of the solution was 29 mmol/L). The enhancement in removal was noted at pH above 2.6, when the carboxylic groups of GLY become negatively charged. At pH > 8, the removal of GLY and AMPA decreases with increasing pH. This effect is more pronounced for AMPA since the overall adsorbed mass is lower for AMPA than for GLY. The hydration layer around GLY and AMPA is thicker and denser at higher pH [87], which requires water molecules to be displaced before contact with the resin surface.

As the pH increases from 4 to 6, the phosphonate group of GLY/AMPA becomes deprotonated, resulting in more negative groups for interaction (electrostatic, ion exchange). However, the increase of pH from 6 to 12 decreases the GLY charge from −2 to −3 and AMPA from −1 to −2, leading to enhancement of the hydration layer around GLY and AMPA molecules. The denser hydration layer inhibits the interaction of GLY/AMPA with the functional groups of the IX resin, thereby reducing the removal. In addition, more hydroxide ions in higher pH solutions also increase the competition for ion-exchange sites on the MIEX surface, interfering with the interaction of GLY and AMPA.

At pH 12 (ionic strength 36 mmol/L), the measured AMPA concentration is surprisingly high – close to or even higher than the initial AMPA concentration in the solution (**Fig. S10**), and simultaneously, the GLY concentration remains low. Since phosphonates are reported to be most stable in the pH range of 3–9 [88], the elevated pH may raise concerns regarding the potential alkaline hydrolysis of GLY to AMPA through C–N bond cleavage. The possibility of GLY degradation to AMPA at high pH was then excluded by experiments with an AMPA-free stock solution at pH 12 (**Fig. S11**), where no AMPA was observed in the 26-h static adsorption process at 20 °C. Other degradation pathways solely due to the highly alkaline conditions are even less probable, as the C–P bond in GLY is highly stable and resistant to strong acid and strong base hydrolysis [23]. Thus, generating other degradation products at extreme pH values is unlikely under the experimental conditions applied. It must be emphasized that the resin used in the experiment was pristine (not previously exposed to GLY or AMPA) and therefore the observed high concentration of AMPA cannot originate from the desorption of the previously adsorbed AMPA.

The pH dependence of GLY and AMPA adsorption highlights the pivotal role of electrostatic interactions in governing IX on MIEX. These interactions are modulated by both the speciation of the micropollutants and their hydration.

3.6. GLY and AMPA removal at increased ionic strength

GLY and AMPA exhibit pH-dependent net charge, and their removal is primarily governed by electrostatic interactions. Consequently, increased ionic strength (I) in the solution can shield electrostatic interactions and inhibit effective ion exchange. Thus, it is essential to investigate if MIEX can still effectively remove GLY and AMPA in high-ionic-strength waters (Fig. 8). The role of ionic strength was investigated across salinities ranging from freshwater and slightly mineralized drinking-water sources (<1 g/L NaCl) to equivalent of brackish waters (20 g/L NaCl) [89]. The experimental parameters (pH and conductivity) and concentration of GLY and AMPA over time in various NaCl

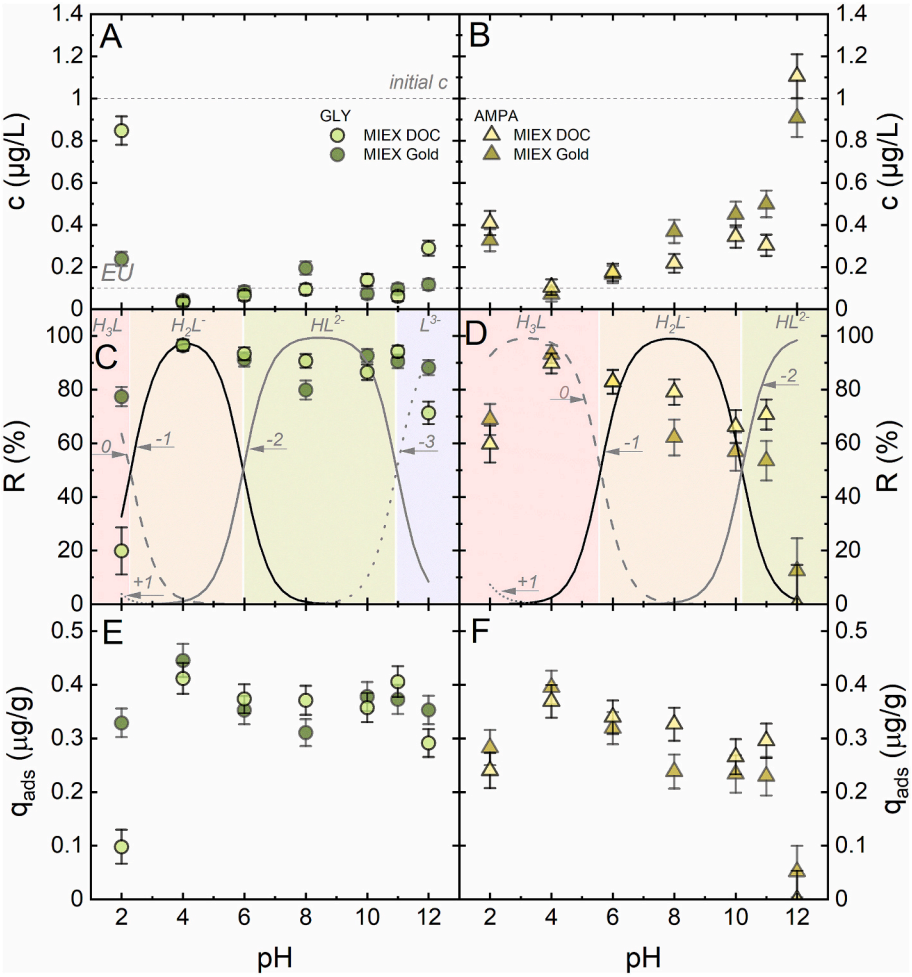

Fig. 6. GLY and AMPA (A-B) concentration (c, µg/L), (C-D) removal (R, %), and (E-F) specific mass adsorbed (q_{ads}, µg/g) on MIEX DOC and MIEX Gold in various pH after 26 h of experiment. The background curves in C-D show the calculated distribution of the predominant protonation species of GLY and AMPA in the corresponding water matrix, obtained using Visual MINTEQ software (v 3.1, KTH, Sweden) [13] (MIEX dose 10 mL/L, initial GLY and AMPA concentration 1 µg/L, 1 mM $NaHCO_3$, 10 mM NaCl, 20 °C, 260 rpm). (For interpretation of the references to colour in this figure legend, the reader is referred to the web version of this article.)

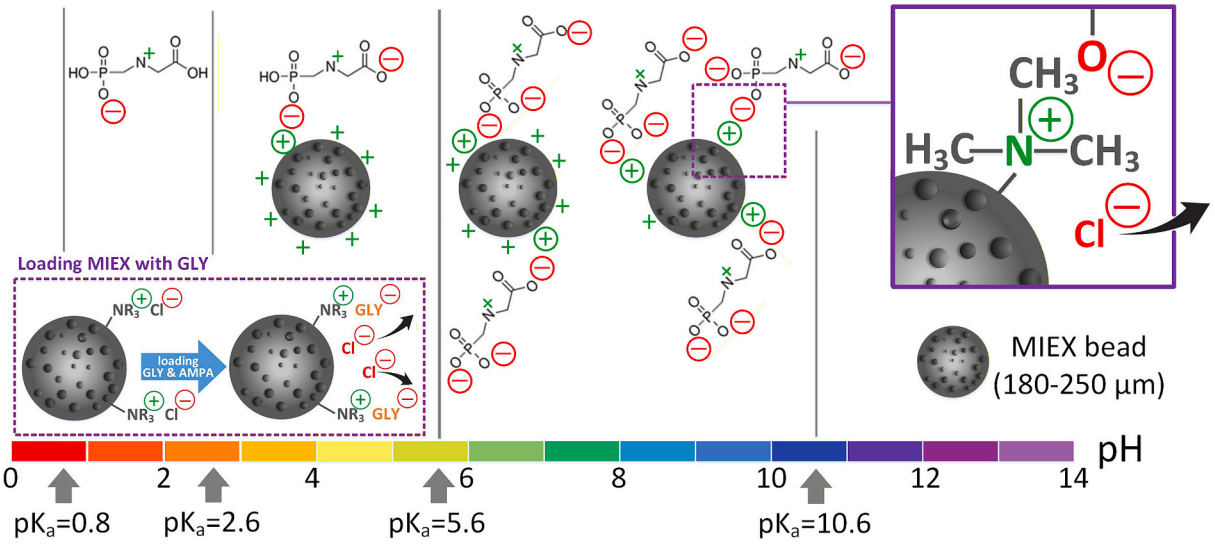

Fig. 7. Ion-dipole interaction of GLY and MIEX in various pH with GLY pK_a values indicated; insets: scheme of replacing chloride anions with negatively charged GLY molecules on the active sites of MIEX. The relative scale between the size of MIEX bead and GLY is not maintained; graphic is intended solely to illustrate the interaction mechanism.

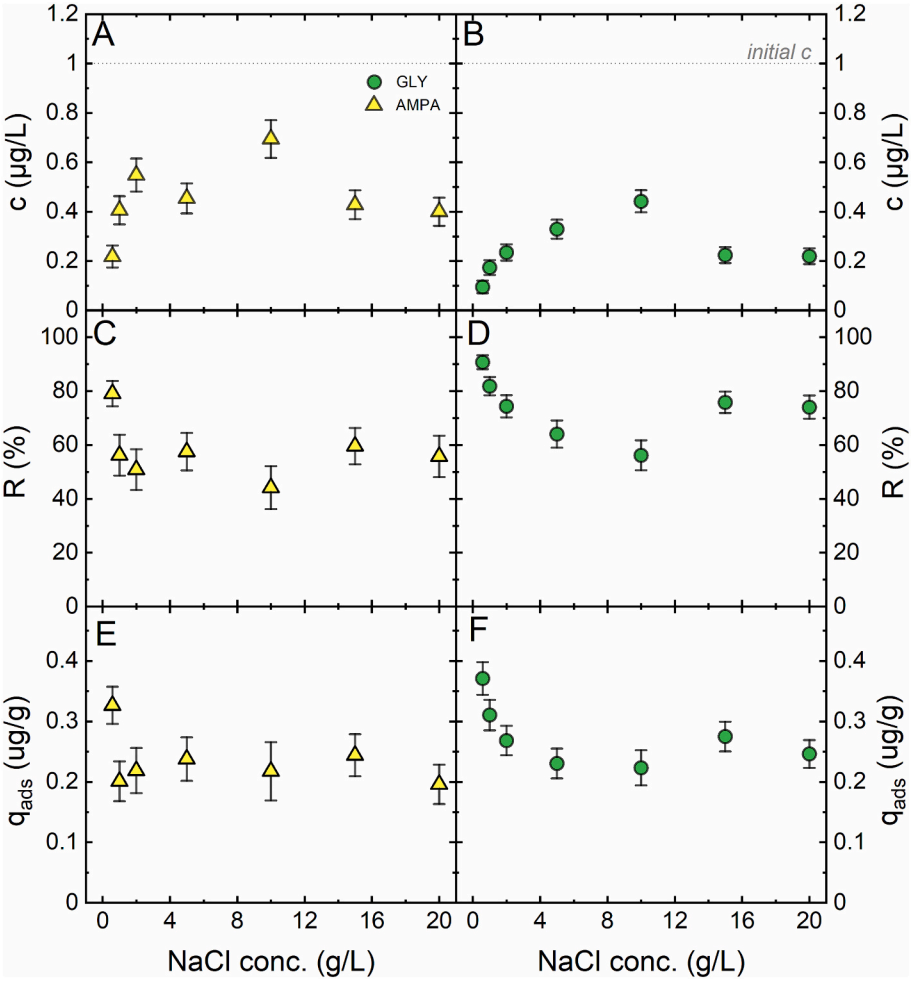

Fig. 8. AMPA and GLY (A-B) concentration, (C-D) removal (R, %), and (E-F) specific mass adsorbed (q_{ads}, µg/g) by MIEX DOC at various NaCl concentration (MIEX DOC dose 10 mL/L, initial GLY and AMPA concentration 1 µg/L, 1 mM $NaHCO_3$, 0–20 g/L NaCl, 20 °C, 260 rpm).

concentrations are presented in **Table S14** and **Fig. S12**.

The removal of GLY and AMPA by MIEX was strongly influenced by ionic strength of the solution, with AMPA exhibiting greater sensitivity than GLY. At low salinity (0.58 g/L NaCl, $I = 11$ mmol/L), the removal of both compounds exceeded 80%. However, increasing NaCl concentration above 1 g/L NaCl ($I = 18$ mmol/L), resulted in the significant drop of the AMPA removal to 55%, whereas GLY removal remained at 65–80% for 5–20 g/L NaCl. Increasing ionic strength compresses the electrical double layer around the positively charged MIEX surface, reducing the Debye length (λ_D) and limiting the effective range of electrostatic interactions to approximately or below 1 nm at moderate to high salinities (**Fig. S13**). As a result, the long-range electrostatic attraction between GLY^-/$AMPA^-$ and positively charged MIEX is screened. The limited changes in removal observed at moderate to high salinities suggest that ion exchange remains the dominant retention mechanism, while short-range interactions (van der Waals interactions and H-bonding) may contribute increasingly under these conditions.

Kinetic parameters of GLY/AMPA adsorption at varying NaCl concentrations are provided in **Table S15** and Fig. 9. The apparent first-order rate constants decreased with increasing ionic strength, particularly for GLY. Together with the observed reduction in removal efficiency, these findings are consistent with a predominantly reversible ion-exchange mechanism.

Consequently, concentrated electrolyte solutions may facilitate desorption and resin regeneration, which is advantageous for high-throughput treatment systems with frequent regeneration cycles. The

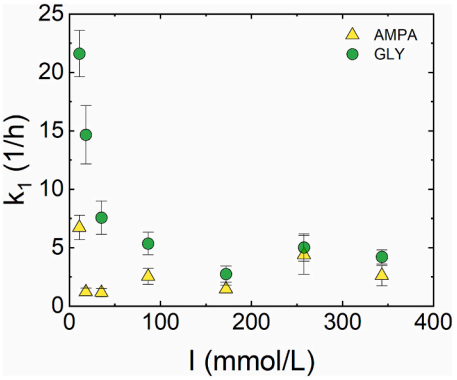

Fig. 9. Apparent first-order rate constant (k_1) for GLY and AMPA adsorption on MIEX DOC as a function of ionic strength (I) within 26 h of the experiment.

increase in NaCl concentration enhances the competitive exchange by background chloride ions. The anion-exchange equilibrium is shifted toward Cl^-, allowing these counter-ions to more easily displace the target GLY^- and $AMPA^-$ species from the resin. Because equilibrium even at high ionic strength was achieved in a short time (**Fig. S12**), the decrease in the GLY/AMPA removal should be attributed primarily to competitive exchange and changes in IX selectivity rather than a kinetic limitations. Irreversible covalent complexation appears to be negligible

in this case. A decrease in micropollutant removal by MIEX with increasing salt concentration was observed in a study on PFAS removal by Gao et al. [60]. Short-chain PFAS (perfluorobutanoic acid, PFBA), containing four carbon atoms (compared to three in GLY), showed a significant 43% reduction in removal with increasing NaCl concentration. The effect of cations has proven to be minor, with the observed competition attributed mainly to chloride ions competing with anionic species for active sites on the resin surface.

In this study, the relatively high GLY removal at 20 g/L NaCl indicates an intrinsic selectivity of MIEX toward GLY as a larger and multivalent anion, which is characteristic of strong-base anion exchangers, compared to monovalent anions such as chloride. The interaction of MIEX DOC with multivalent anions was ranked in the study by Yang et al., with monovalent ions (Cl^-) at the lowest and divalent ions at the highest [90]. Although the ion exchange remains the dominant mechanism, the contribution from secondary interactions within the polymeric matrix (such as van der Waals forces or H-bonding) cannot be entirely excluded.

3.7. Interpretation of GLY/AMPA adsorption on MIEX

Taken together, the results obtained under varying solution chemistry and adsorption conditions provide a coherent picture of the physicochemical interactions governing GLY and AMPA removal by MIEX. The observed adsorption behavior can be rationalized by the interplay between electrostatic interactions, ion exchange, molecular speciation, and hydration, which together determine the accessibility and affinity of GLY and AMPA toward the resin.

In aqueous systems, GLY/AMPA molecules are transported from the bulk toward MIEX (i) and diffuse through the boundary layer around the MIEX bead (ii). Then GLY/AMPA diffuses inward through the pores of MIEX to IX sites (iii). When GLY approaches the MIEX surface, electrostatic attraction (considered a long-range force) facilitates its transport and brings negatively charged GLY into the vicinity of the positively charged MIEX surface, thereby enabling ion exchange (iv). Once GLY is within the molecular contact range, complementary short-range interactions (<1 nm), such as hydrogen bonding and van der Waals interactions, may contribute to the adsorption of GLY and AMPA. Following the ion exchange, the exchanged ions diffuse outward through the pores toward the surface (v), and then diffuse through the liquid film or boundary layer (vi) to finally move into the bulk (vii). In a stirred batch process, the overall rate is controlled by (ii) film diffusion and (iii) pore diffusion [91].

The removal of ionic herbicide bentazone by MIEX has been investigated previously, with ion exchange identified as the primary removal mechanism [18]. Bentazone occurs predominantly as an anion above its pK_a of 3.3 and, unlike GLY, has a hydrophobic aromatic moiety. The presence of a hydrophobic aromatic moiety may promote additional interactions with the resin matrix, which has been suggested to contribute to the higher sorption capacity of MIEX for bentazone compared to GLY [18]. Another ionizable herbicide, 2,4-dichlorophenoxyacetic acid, is a small molecule with an aromatic moiety whose removal from water was attributed primarily to ion exchange interactions enhanced by adsorption to the resin matrix [92]. In contrast to bentazone and 2,4-dichlorophenoxyacetic acid, which contain hydrophobic aromatic moieties, GLY is a highly polar molecule that exists predominantly as a multi-charged anion under environmentally relevant pH conditions. The resulting strong hydration and lack of hydrophobic domains limit additional adsorption interactions with MIEX and make GLY more challenging to remove from water.

Specific and non-specific interactions with MIEX have previously been reported for the steroid hormone micropollutant estrone [43]. Below its pK_a of 10.4, predominantly neutral and polar estrone can be removed by MIEX primarily through the physical interactions (van der Waals forces and hydrogen bonding) with the polyacrylate MIEX matrix, resulting in a moderate removal of 40% from the initial concentrations up to 500 ng/L. At pH above 10.4, when estrone is predominantly negatively charged, removal by MIEX increased to 70% due to the dominant ion exchange mechanism in these conditions. This example demonstrates that even in the absence of electrostatic attraction, physical interactions with the resin matrix can contribute substantially to micropollutant removal.

The MIEX resin regeneration is carried out in the desorption process using 10–12% w/w NaCl [46,56]. In high chloride concentration, ions sorbed to the quaternary ammonium site are substituted for chloride ions, which exhibit a strong affinity for the exchange site. The concentration of 100 g/L NaCl typically used for MIEX resin regeneration would provide a much stronger chemical driving force (and significantly larger molar excess of Cl^- over GLY^-) than 20 g/L used in the experiments. The observed sensitivity of adsorption kinetics and removal efficiency to ionic strength is consistent with the regeneration strategy employed for MIEX. Performing the laboratory-scale tests of the regeneration effectiveness of the IX resin over a limited number of cycles and extrapolating the results to the larger-scale installations should be interpreted with caution.

It can be expected that MIEX may, to some extent, retain GLY and AMPA within the polymeric matrix through non-ion-exchange interactions (electrostatic interactions, H-bonding, van der Waals interactions). These fractions may not be fully removed during the regeneration in NaCl, leading to gradual accumulation within the resin and potential release upon changes in solution conditions [43].

IX resins have been previously applied for the removal of micropollutants from wastewater, but within the concentration range of micropollutants present in drinking water, the number of reports is lower [38]. The present study, conducted in well-defined synthetic matrices, provides a foundation for understanding the removal of GLY and AMPA by the MIEX resin. However, further investigations in natural water matrices are necessary, as interactions with organic matter and competing ions are expected to significantly influence the real-world performance of MIEX toward GLY and AMPA.

4. Conclusions

MIEX could remove GLY and AMPA at environmentally relevant concentrations, with 10 mL/L identified as the critical resin dose, which is comparable to doses used in full-scale water treatment. However, the EU guideline for individual herbicide (100 ng/L) was not achieved. Further optimization of the MIEX dose and operating conditions may improve GLY and AMPA removal. Alternatively, MIEX could be integrated into a hybrid treatment process, for example with membrane filtration, and the potential of such an approach to further reduce GLY and AMPA concentrations toward the ng/L range could be investigated. The findings indicate that GLY and AMPA removal by MIEX is primarily controlled by electrostatically driven ion exchange and the accessibility of ion-exchange sites. Solution chemistry strongly influences the affinity of GLY and AMPA toward MIEX. Enhanced performance was observed at pH 4–10 and low ionic strength, resulting from the combined influence of GLY/AMPA speciation, electrostatic screening, competition from background ions for IX sites, and molecular hydration. While electrostatic interactions dominate the removal process, secondary interactions within the polymeric matrix, including van der Waals forces and hydrogen bonding, may also contribute. Adsorption kinetics and the accessibility of exchange sites were found to play a major role in determining performance, indicating that equilibrium adsorption capacity alone may not provide a sufficient basis for evaluating adsorbents intended for short-contact applications (such as inline slurry contactors or hybrid systems with filtration membranes).

The results demonstrate that MIEX is a promising option for removal of environmentally relevant concentrations of GLY and AMPA from low-salinity waters, where electrostatic interactions remain effective and competition from background ions is limited, offering operational advantages such as rapid adsorption and suitability for slurry-phase

operation with magnetic separation. The relatively straightforward regeneration of the resin further supports the applicability of MIEX in cyclic treatment-regeneration processes such as completely mixed or fluidized bed reactor systems. The knowledge gained from the static adsorption experiments forms a basis for translating laboratory findings into practical applications and enables meaningful comparison of adsorption performance across different adsorbents.

CRediT authorship contribution statement

Martyna Krajewska: Writing – original draft, Visualization, Validation, Investigation, Data curation, Conceptualization. **Phuong B. Trinh:** Writing – review & editing, Writing – original draft, Validation, Investigation. **Andrea I. Schäfer:** Writing – review & editing, Validation, Supervision, Resources, Funding acquisition, Conceptualization.

Declaration of competing interest

The authors declare that they have no known competing financial interests or personal relationships that could have appeared to influence the work reported in this paper.

Acknowledgements

The Helmholtz Association Recruitment Initiative is thanked for IAMT funding. Deutscher Akademischer Austauschdienst (DAAD) has provided a PhD scholarship for P.B.T (program ID 57440921). IXOM is thanked for supplying MIEX and Perkin Elmer for assistance with the LC-MS/MS instrument maintenance. Minh N. Nguyen (IAMT) is acknowledged for his assistance in the laboratory and discussions, revision and feedback, and Alessandra Imbrogno (IAMT) for inspiring the direction of this research. The Open Access funding was enabled and organized by Project DEAL.

Appendix A. Supplementary data

Supplementary data to this article can be found online at https://doi.org/10.1016/j.jwpe.2026.110868.

Data availability

Data will be made available on request.

References

[1] F.S. Galli, M. Mollari, V. Tassinari, C. Alimonti, A. Ubaldi, C. Cuva, D. Marcoccia, Overview of human health effects related to glyphosate exposure, Front. Toxicol. 6 (2024) 1474792, https://doi.org/10.3389/ftox.2024.1474792.
[2] F. Mendez, J. Ordoñez-Betancourth, N. Abrahams, Effects of glyphosate exposure on reproductive health: a systematic review of human, animal and in-vitro studies, Expo. Health 14 (2022) 635–669, https://doi.org/10.1007/s12403-021-00442-4.
[3] G.M. Williams, R. Kroes, I.C. Munro, Safety evaluation and risk assessment of the herbicide roundup and its active ingredient, glyphosate, for humans, Regul. Toxicol. Pharmacol. 31 (2000) 117–165, https://doi.org/10.1006/rtph.1999.1371.
[4] G.M. Williams, R. Kroes, I.C. Munro, Retraction notice to "Safety evaluation and risk assessment of the herbicide roundup and its active ingredient, glyphosate, for humans"[Regul. Toxicol. Pharm. 31 (2000) 117–165], Regul. Toxicol. Pharmacol. (2025) 106006, https://doi.org/10.1016/j.yrtph.2025.106006.
[5] L. Parra-Arroyo, R.B. González-González, C. Castillo-Zacarías, E.M.M. Martínez, J. E. Sosa-Hernández, M. Bilal, H.M. Iqbal, D. Barceló, R. Parra-Saldívar, Highly hazardous pesticides and related pollutants: toxicological, regulatory, and analytical aspects, Sci. Total Environ. 807 (2022) 151879, https://doi.org/10.1016/j.scitotenv.2021.151879.
[6] M. Schwientek, H. Rügner, S. Haderlein, W. Schulz, B. Wimmer, L. Engelbart, S. Bieger, C. Huhn, Glyphosate contamination in European rivers not from herbicide application? Water Res. 263 (2024) 122140 https://doi.org/10.1016/j.watres.2024.122140.
[7] J.P. Muñoz, E. Silva-Pavez, D. Carrillo-Beltrán, G.M. Calaf, Occurrence and exposure assessment of glyphosate in the environment and its impact on human beings, Environ. Res. 231 (2023) 116201, https://doi.org/10.1016/j.envres.2023.116201.
[8] N. Suciu, E. Russo, M. Calliera, G.P. Luciani, M. Trevisan, E. Capri, Glyphosate, glufosinate ammonium, and AMPA occurrences and sources in groundwater of hilly vineyards, Sci. Total Environ. 866 (2023) 161171, https://doi.org/10.1016/j.scitotenv.2022.161171.
[9] The European Parliament and the Council of European Union, Directive (EU) 2020/2184 of the European parliament and of the council of 16 December 2020 on the quality of water intended for human consumption. https://eur-lex.europa.eu/legal-content/EN/TXT/HTML/?uri=CELEX:32020L2184, 2020. (Accessed 22 April 2026).
[10] The European Comission, Comission implementing regulation (EU) 2023/2660. https://eur-lex.europa.eu/legal-content/EN/TXT/PDF/?uri=OJ:L_202302660, 2023. (Accessed 21 February 2024).
[11] Bund/Länder-Arbeitsgemeinschaft Wasser (LAWA) unter dem Vorsitz des Ministeriums für Landwirtschaft Umwelt und Klimaschutz des Landes Brandenburg, Bericht zur Grundwasserbeschaffenheit in Deutschland Pflanzenschutzmittelwirkstoffe und Metaboliten Funde und Tendenzen Berichtszeitraum 2017 bis 2021. https://www.lawa.de/documents/psm-bericht-2023-12-22-barrierearm-final_2_1728974845.pdf, 2024. (Accessed 7 November 2025).
[12] P.B. Trinh, A.I. Schäfer, Removal of glyphosate (GLY) and aminomethylphosphonic acid (AMPA) by ultrafiltration with permeate-side polymer-based spherical activated carbon (UF–PBSAC), Water Res. 250 (2024) 121021, https://doi.org/10.1016/j.watres.2023.121021.
[13] P.B. Trinh, A.I. Schäfer, Adsorption of glyphosate and metabolite aminomethylphosphonic acid (AMPA) from water by polymer-based spherical activated carbon (PBSAC), J. Hazard. Mater. 454 (2023) 131211, https://doi.org/10.1016/j.jhazmat.2023.131211.
[14] N. Hosseini, M.R. Toosi, Removal of 2,4-D, glyphosate, trifluralin, and butachlor herbicides from water by polysulfone membranes mixed by graphene oxide/TiO_2 nanocomposite: study of filtration and batch adsorption, J. Environ. Health Sci. Eng. 17 (2019) 247–258, https://doi.org/10.1007/s40201-019-00344-3.
[15] Z. Liu, M. Xie, F. Ni, Y. Xu, Nanofiltration process of glyphosate simulated wastewater, Water Sci. Technol. 65 (2012) 816–822, https://doi.org/10.2166/wst.2012.808.
[16] C.A. Villamar-Ayala, J.V. Carrera-Cevallos, R. Vasquez-Medrano, P.J. Espinoza-Montero, Fate, eco-toxicological characteristics, and treatment processes applied to water polluted with glyphosate: a critical review, Crit. Rev. Environ. Sci. Technol. 49 (2019) 1476–1514, https://doi.org/10.1080/10643389.2019.1579627.
[17] M. Rigobello-Masini, E.A.O. Pereira, G. Abate, J.C. Masini, Solid-phase extraction of glyphosate in the analyses of environmental, plant, and food samples, Chromatographia 82 (2019) 1121–1138, https://doi.org/10.1007/s10337-019-03748-3.
[18] Z. Liu, X. Yan, M. Drikas, D. Zhou, D. Wang, M. Yang, J. Qu, Removal of bentazone from micro-polluted water using MIEX resin: kinetics, equilibrium, and mechanism, J. Environ. Sci. 23 (2011) 381–387, https://doi.org/10.1016/s1001-0742(10)60441-x.
[19] H. Saitúa, F. Giannini, A.P. Padilla, Drinking water obtaining by nanofiltration from waters contaminated with glyphosate formulations: process evaluation by means of toxicity tests and studies on operating parameters, J. Hazard. Mater. 227 (2012) 204–210, https://doi.org/10.1016/j.jhazmat.2012.05.035.
[20] Directive 2000/60/EC of the European Parliament and of the Council of 23 October 2000 establishing a framework for Community action in the field of water policy. https://eur-lex.europa.eu/resource.html?uri=cellar:5c835afb-2ec6-4577-bdf8-756d3d694eeb.0004.02/DOC_1&format=PDF, 2000. (Accessed 21 February 2024).
[21] S.O. Duke, Glyphosate: environmental fate and impact, Weed Sci. 68 (2020) 201–207, https://doi.org/10.1017/wsc.2019.28.
[22] A.M. Muskus, M. Krauss, A. Miltner, U. Hamer, K.M. Nowak, Degradation of glyphosate in a Colombian soil is influenced by temperature, total organic carbon content and pH, Environ. Pollut. 259 (2020) 113767, https://doi.org/10.1016/j.envpol.2019.113767.
[23] D.P. Jaisi, H. Li, A.F. Wallace, P. Paudel, M. Sun, A. Balakrishna, R.N. Lerch, Mechanisms of bond cleavage during manganese oxide and UV degradation of glyphosate: results from phosphate oxygen isotopes and molecular simulations, J. Agric. Food Chem. 64 (2016) 8474–8482, https://doi.org/10.1021/acs.jafc.6b02608.
[24] V.B.K. Yaah, S. Ahmadi, J. Quimbayo, S. Morales-Torres, S. Ojala, Recent technologies for glyphosate removal from aqueous environment: a critical review, Environ. Res. 240 (2024) 117477, https://doi.org/10.1016/j.envres.2023.117477.
[25] J. Jönsson, R. Camm, T. Hall, Removal and degradation of glyphosate in water treatment: a review, J. Water Supply Res. Technol. AQUA 62 (2013) 395–408, https://doi.org/10.2166/aqua.2013.080.
[26] A. Mehrsheikh, M. Bleeke, S. Brosillon, A. Laplanche, P. Roche, Investigation of the mechanism of chlorination of glyphosate and glycine in water, Water Res. 40 (2006) 3003–3014, https://doi.org/10.1016/j.watres.2006.06.027.
[27] H. Lan, Z. Jiao, X. Zhao, W. He, A. Wang, H. Liu, R. Liu, J. Qu, Removal of glyphosate from water by electrochemically assisted MnO_2 oxidation process, Sep. Purif. Technol. 117 (2013) 30–34, https://doi.org/10.1016/j.seppur.2013.04.012.
[28] W. Xue, G. Zhang, X. Xu, X. Yang, C. Liu, Y. Xu, Preparation of titania nanotubes doped with cerium and their photocatalytic activity for glyphosate, Chem. Eng. J. 167 (2011) 397–402, https://doi.org/10.1016/j.cej.2011.01.007.
[29] H. Lan, W. He, A. Wang, R. Liu, H. Liu, J. Qu, C.P. Huang, An activated carbon fiber cathode for the degradation of glyphosate in aqueous solutions by the electro-Fenton mode: optimal operational conditions and the deposition of iron on cathode on electrode reusability, Water Res. 105 (2016) 575–582, https://doi.org/10.1016/j.watres.2016.09.036.

[30] A. Serra-Clusellas, L. De Angelis, M. Beltramo, M. Bava, J. De Frankenberg, J. Vigliarolo, N. Di Giovanni, J.D. Stripeikis, J.A. Rengifo-Herrera, M.M. Fidalgo de Cortalezzi, Glyphosate and AMPA removal from water by solar induced processes using low Fe(III) or Fe(II) concentrations, Environ. Sci.: Water Res. Technol. 5 (2019) 1932–1942, https://doi.org/10.1039/C9EW00442D.
[31] J. Yuan, J. Duan, C.P. Saint, D. Mulcahy, Removal of glyphosate and aminomethylphosphonic acid from synthetic water by nanofiltration, Environ. Technol. 39 (2018) 1384–1392, https://doi.org/10.1080/09593330.2017.1329356.
[32] J.C. Diel, K. da Boit Martinello, C.L. da Silveira, H.A. Pereira, D.S. Franco, L. F. Silva, G.L. Dotto, New insights into glyphosate adsorption on modified carbon nanotubes via green synthesis: statistical physical modeling and steric and energetic interpretations, Chem. Eng. J. 431 (2022) 134095, https://doi.org/10.1016/j.cej.2021.134095.
[33] Y.S. Hu, Y.Q. Zhao, B. Sorohan, Removal of glyphosate from aqueous environment by adsorption using water industrial residual, Desalination 271 (2011) 150–156, https://doi.org/10.1016/j.desal.2010.12.014.
[34] S.S. Mayakaduwa, P. Kumarathilaka, I. Herath, M. Ahmad, M. Al-Wabel, Y.S. Ok, A. Usman, A. Abduljabbar, M. Vithanage, Equilibrium and kinetic mechanisms of woody biochar on aqueous glyphosate removal, Chemosphere 144 (2016) 2516–2521, https://doi.org/10.1016/j.chemosphere.2015.07.080.
[35] G. Xiao, R. Wen, Comparative adsorption of glyphosate from aqueous solution by 2-aminopyridine modified polystyrene resin, D301 resin and 330 resin: influencing factors, salinity resistance and mechanism, Fluid Phase Equilib. 411 (2016) 1–6, https://doi.org/10.1016/j.fluid.2015.11.026.
[36] Q. Chen, J. Zheng, Q. Yang, Z. Dang, L. Zhang, Insights into the glyphosate adsorption behavior and mechanism by a $MnFe_2O_4$@cellulose-activated carbon magnetic hybrid, ACS Appl. Mater. Interfaces 11 (2019) 15478–15488, https://doi.org/10.1021/acsami.8b22386.
[37] B. Böhringer, O. Guerra Gonzalez, I. Eckle, M. Müller, J.M. Giebelhausen, C. Schrage, S. Fichtner, Polymer-based spherical activated carbons - from adsorptive properties to filter performance, Chem. Ing. Tech. 83 (2011) 53–60, https://doi.org/10.1002/cite.201000166.
[38] M. Haddad, C. Oie, S.V. Duy, S. Sauvé, B. Barbeau, Adsorption of micropollutants present in surface waters onto polymeric resins: impact of resin type and water matrix on performance, Sci. Total Environ. 660 (2019) 1449–1458, https://doi.org/10.1016/j.scitotenv.2018.12.247.
[39] J. Bensalah, A. Thakur, A. Kumar, Investigating the adsorption processes of polymer resins for the removal of micropollutants: a comprehensive review in the field of environmental remediation, Environ. Res. 254 (2024) 119128, https://doi.org/10.1016/j.envres.2024.119128.
[40] T.H. Boyer, Y. Fang, A. Ellis, R. Dietz, Y.J. Choi, C.E. Schaefer, C.P. Higgins, T. J. Strathmann, Anion exchange resin removal of per-and polyfluoroalkyl substances (PFAS) from impacted water: a critical review, Water Res. 200 (2021) 117244, https://doi.org/10.1016/j.watres.2021.117244.
[41] S.M. Bannon, G.M. Geise, Influence of Donnan and dielectric exclusion on ion sorption in sulfonated polysulfones, J. Membr. Sci. 694 (2024) 122396, https://doi.org/10.1016/j.memsci.2023.122396.
[42] I. Levchuk, J.J.R. Màrquez, M. Sillanpää, Removal of natural organic matter (NOM) from water by ion exchange – a review, Chemosphere 192 (2018) 90–104, https://doi.org/10.1016/j.chemosphere.2017.10.101.
[43] P.A. Neale, M. Mastrup, T. Borgmann, A.I. Schäfer, Sorption of micropollutant estrone to a water treatment ion exchange resin, J. Environ. Monit. 12 (2010) 311–317, https://doi.org/10.1039/b913338k.
[44] M. Mołczan (Ed.), Parametry procesu wymiany anionowej na proszkowych adsorbentach magnetycznych jako narzedzie kontroli usuwania naturalnych substancji organicznych z wody, Oficyna Wydawnicza Politechniki Wrocławskiej, Wrocław, 2019. ISBN 978-83-7493-081-9.
[45] A. Imbrogno, A. Tiraferri, S. Abbenante, S. Weyand, R. Schwaiger, T. Luxbacher, A. I. Schäfer, Organic fouling control through magnetic ion exchange-nanofiltration (MIEX-NF) in water treatment, J. Membr. Sci. 549 (2018) 474–485, https://doi.org/10.1016/j.memsci.2017.12.041.
[46] M. Slunjski, K. Cadee, J. Tattersall, MIEX® resin water treatment process, in: Proceedings of Aquatech 26, 2000, p. 29.
[47] M. Kalaruban, P. Loganathan, W. Shim, J. Kandasamy, G. Naidu, T.V. Nguyen, S. Vigneswaran, Removing nitrate from water using iron-modified Dowex 21K XLT ion exchange resin: batch and fluidised-bed adsorption studies, Sep. Purif. Technol. 158 (2016) 62–70, https://doi.org/10.1016/j.seppur.2015.12.022.
[48] M. Chabani, A. Amrane, A. Bensmaili, Equilibrium sorption isotherms for nitrate on resin Amberlite IRA 400, J. Hazard. Mater. 165 (2009) 27–33, https://doi.org/10.1016/j.jhazmat.2008.08.091.
[49] Y. Jia, L. Ding, P. Ren, M. Zhong, J. Ma, X. Fan, Performances and mechanism of methyl orange and Congo red adsorbed on the magnetic ion-exchange resin, J. Chem. Eng. Data 65 (2020) 725–736, https://doi.org/10.1021/acs.jced.9b00951.
[50] C. Shuang, P. Li, A. Li, Q. Zhou, M. Zhang, Y. Zhou, Quaternized magnetic microspheres for the efficient removal of reactive dyes, Water Res. 46 (2012) 4417–4426, https://doi.org/10.1016/j.watres.2012.05.052.
[51] H. Humbert, H. Gallard, H. Suty, J.-P. Croué, Performance of selected anion exchange resins for the treatment of a high DOC content surface water, Water Res. 39 (2005) 1699–1708, https://doi.org/10.1016/j.watres.2005.02.008.
[52] C.M. López-Ortiz, I. Sentana-Gadea, P. Varó-Galvañ, S.E. Maestre-Pérez, D. Prats-Rico, The use of combined treatments for reducing parabens in surface waters: ion-exchange resin and nanofiltration, Sci. Total Environ. 639 (2018) 228–236, https://doi.org/10.1016/j.scitotenv.2018.05.150.
[53] M. Mołczan, The new concept of MIEX® resin dose categories. Swelling effect, reactor steady-state balance, and NOM removal process control, Environ. Prot. Eng. 50 (2024), https://doi.org/10.37190/epe240105.
[54] M. Park, K.D. Daniels, S. Wu, A.D. Ziska, S.A. Snyder, Magnetic ion-exchange (MIEX) resin for perfluorinated alkylsubstance (PFAS) removal in groundwater: roles of atomic charges for adsorption, Water Res. 181 (2020) 115897, https://doi.org/10.1016/j.watres.2020.115897.
[55] S.E. Comstock, T.H. Boyer, Combined magnetic ion exchange and cation exchange for removal of DOC and hardness, Chem. Eng. J. 241 (2014) 366–375, https://doi.org/10.1016/j.cej.2013.10.073.
[56] P.A. Neale, A. Schäfer, Magnetic ion exchange: is there potential for international development? Desalination 248 (2009) 160–168, https://doi.org/10.1016/j.desal.2008.05.052.
[57] M. Drikas, M. Dixon, J. Morran, Long term case study of MIEX pre-treatment in drinking water; understanding NOM removal, Water Res. 45 (2011) 1539–1548, https://doi.org/10.1016/j.watres.2010.11.024.
[58] M. Rajca, A. Włodyka-Bergier, M. Bodzek, T. Bergier, MIEX® DOC process to remove disinfection by-product precursors, Desalin. Water Treat. 64 (2017) 372–377, https://doi.org/10.5004/dwt.2017.11397.
[59] P. Jutaporn, P.C. Singer, R.M. Cory, O. Coronell, Minimization of short-term low-pressure membrane fouling using a magnetic ion exchange (MIEX®) resin, Water Res. 98 (2016) 225–234, https://doi.org/10.1016/j.watres.2016.04.007.
[60] Y. Gao, S.-T. Le, J. Hou, J. McDonald, A. Colusso, M.J. Lee, M. Raymond, B. Oldland, C. Smith, M. Roehl, P. Griffits, S. Khan, T.C.G. Kibbey, D.M. O'Carroll, Prediction of the impact of hydrochemistry on PFAS removal using ion exchange resins, ACS EST Water 5 (2025) 6353–6364, https://doi.org/10.1021/acsestwater.5c00499.
[61] A.M. Smith, A.A. Lee, S. Perkin, The electrostatic screening length in concentrated electrolytes increases with concentration, J. Phys. Chem. Lett. 7 (2016) 2157–2163, https://doi.org/10.1021/acs.jpclett.6b00867.
[62] Y. Gao, W. Wu, L. Shen, J. Qu, Y. Li, D. Sun, Z. Dong, L. Ding, Adsorption behavior and mechanism insight of organoarsenic compounds on magnetic ion exchange resin based on the combined method of DFT calculation and characterization, J. Water Process Eng. 70 (2025) 107029, https://doi.org/10.1016/j.jwpe.2025.107029.
[63] A.J. Neel, M.J. Hilton, M.S. Sigman, F.D. Toste, Exploiting non-covalent π interactions for catalyst design, Nature 543 (2017) 637–646, https://doi.org/10.1038/nature21701.
[64] P. Jutaporn, N. Muenphukhiaw, P. Phungsai, S. Leungprasert, C. Musikavong, Characterization of DBP precursor removal by magnetic ion exchange resin using spectroscopy and high-resolution mass spectrometry, Water Res. 217 (2022) 118435, https://doi.org/10.1016/j.watres.2022.118435.
[65] T.R. Santos, M.B. Andrade, M.F. Silva, R. Bergamasco, S. Hamoudi, Development of α-and γ-Fe_2O_3 decorated graphene oxides for glyphosate removal from water, Environ. Technol. 40 (2019) 1118–1137, https://doi.org/10.1080/09593330.2017.1411397.
[66] H. Park, A. May, L. Portilla, H. Dietrich, F. Münch, T. Rejek, M. Sarcletti, L. Banspach, D. Zahn, M. Halik, Magnetite nanoparticles as efficient materials for removal of glyphosate from water, Nat. Sustainability 3 (2020) 129–135, https://doi.org/10.1038/s41893-019-0452-6.
[67] V.O.S. Sousa Neto, G.S.C. Raulino, P.T.C. Freire, M.A. Araújo-Silva, R.F. do Nascimento, Equilibrium and kinetic studies in adsorption of toxic metal ions for wastewater treatment, in: M. Naushad, Z.A. Al-Othman (Eds.), A Book on Ion Exchange, Adsorption and Solvent Extraction, Nova Science Publishers, Inc., Hauppauge, NY, USA, 2013, pp. 145–182. ISBN 978-1-62417-887-0.
[68] S. Rahmani, M. Mohseni, The role of hydrophobic properties in ion exchange removal of organic compounds from water, Can. J. Chem. Eng. 95 (2017) 1449–1455, https://doi.org/10.1002/cjce.22823.
[69] P. Finkbeiner, G. Moore, T. Tseka, T.T. Nkambule, L.D. Kock, B. Jefferson, P. Jarvis, Interactions between organic model compounds and ion exchange resins, Environ. Sci. Technol. 53 (2019) 9734–9743, https://doi.org/10.1021/acs.est.9b02139.
[70] IXOM WATERCARE, MIEX DOC resin safety data sheet. https://www.ixomwatercare.com/documents/sds-eu-miex-doc-resin/download, 2017. (Accessed 7 February 2024).
[71] IXOM WATERCARE, MIEX Gold resin safety data sheet. https://www.ixomwatercare.com/documents/sds-eu-miex-gold-resin/download, 2017. (Accessed 7 February 2024).
[72] R. Hans, G. Senanayake, L. Dharmasiri, J. Mathes, D. Kim, A preliminary batch study of sorption kinetics of Cr (VI) ions from aqueous solutions by a magnetic ion exchange (MIEX®) resin and determination of film/pore diffusivity, Hydrometallurgy 164 (2016) 208–218, https://doi.org/10.1016/j.hydromet.2016.06.007.
[73] M. Tagliavini, F. Engel, P.G. Weidler, T. Scherer, A.I. Schäfer, Adsorption of steroid micropollutants on polymer-based spherical activated carbon (PBSAC), J. Hazard. Mater. 337 (2017) 126–137, https://doi.org/10.1016/j.jhazmat.2017.03.036.
[74] P. Jutaporn, M. Armstrong, O. Coronell, Assessment of C-DBP and N-DBP formation potential and its reduction by MIEX® DOC and MIEX® GOLD resins using fluorescence spectroscopy and parallel factor analysis, Water Res. 172 (2020) 115460, https://doi.org/10.1016/j.watres.2019.115460.
[75] M. Soyluoglu, M.S. Ersan, M. Ateia, T. Karanfil, Removal of bromide from natural waters: bromide-selective vs. conventional ion exchange resins, Chemosphere 238 (2020) 124583, https://doi.org/10.1016/j.chemosphere.2019.124583.
[76] T.H. Boyer, Removal of dissolved organic matter by magnetic ion exchange resin, Curr. Pollut. Rep. 1 (2015) 142–154, https://doi.org/10.1007/s40726-015-0012-2.

[77] T. Tamanna, P.J. Mahon, R.K. Hockings, H. Alam, M. Raymond, C. Smith, C. Clarke, A. Yu, Ion exchange MIEX® GOLD resin as a promising sorbent for the removal of PFAS compounds, Appl. Sci. 13 (2023) 6263, https://doi.org/10.3390/app13106263.
[78] A. Gibson, S. Golubovic, MIEX gold resin: demonstration at Aireys Inlet, Water J. 42 (2015) 50–52.
[79] C. López-Ortiz, I. Sentana-Gadea, P.J. Varó-Galvañ, S. Maestre-Pérez, D. Prats-Rico, Effect of magnetic ion exchange (MIEX®) on removal of emerging organic contaminants, Chemosphere 208 (2018) 433–440, https://doi.org/10.1016/j.chemosphere.2018.05.194.
[80] C. Yao, T. Chen, A new simplified method for estimating film mass transfer and surface diffusion coefficients from batch adsorption kinetic data, Chem. Eng. J. 265 (2015) 93–99, https://doi.org/10.1016/j.cej.2014.12.005.
[81] Z. Zhu, M. Zhang, F. Liu, C. Shuang, C. Zhu, Y. Zhang, A. Li, Effect of polymeric matrix on the adsorption of reactive dye by anion-exchange resins, J. Taiwan Inst. Chem. Eng. 62 (2016) 98–103, https://doi.org/10.1016/j.jtice.2016.01.017.
[82] P. Krzeminski, C. Vogelsang, T. Meyn, S. Köhler, H. Poutanen, H. De Wit, W. Uhl, Natural organic matter fractions and their removal in full-scale drinking water treatment under cold climate conditions in Nordic capitals, J. Environ. Manag. 241 (2019) 427–438, https://doi.org/10.1016/j.jenvman.2019.02.024.
[83] J.P. Vareda, On validity, physical meaning, mechanism insights and regression of adsorption kinetic models, J. Mol. Liq. 376 (2023) 121416, https://doi.org/10.1016/j.molliq.2023.121416.
[84] S.P. Lenka, M. Kah, J.L.-Y. Chen, B.A. Tiban-Anrango, L.P. Padhye, Adsorption mechanisms of short-chain and ultrashort-chain PFAS on anion exchange resins and activated carbon, Environ. Sci.: Water Res. Technol. 10 (2024) 1280–1293, https://doi.org/10.1039/d3ew00959a.
[85] J. Wang, X. Guo, Adsorption isotherm models: classification, physical meaning, application and solving method, Chemosphere 258 (2020) 127279, https://doi.org/10.1016/j.chemosphere.2020.127279.
[86] M. Song, M. Li, Adsorption and regeneration characteristics of phosphorus from sludge dewatering filtrate by magnetic anion exchange resin, Environ. Sci. Pollut. Res. 26 (2019) 34233–34247, https://doi.org/10.1007/s11356-018-4049-9.
[87] P.B. Trinh, M. Nguyen, Z. Futera, B. Minofar, M. Personeni, P. Petersen, A. I. Schäfer, The role of hydration in the removal of glyphosate (GLY) and aminomethylphosphonic acid (AMPA) by nanofiltration membranes, Nat. Commun. 17 (2026), https://doi.org/10.1038/s41467-026-71492-y.
[88] J.F. Villarreal-Chiu, A.G. Acosta-Cortés, S. Kumar, G. Kaushik, Biological limitations on glyphosate biodegradation, in: R. Singh, S. Kumar (Eds.), Green Technologies and Environmental Sustainability, Springer International Publishing, Cham, 2017, pp. 179–201, 978-3-319-50654-8.
[89] J.R. Du, X. Zhang, X. Feng, Y. Wu, F. Cheng, M.E. Ali, Desalination of high salinity brackish water by an NF-RO hybrid system, Desalination 491 (2020) 114445, https://doi.org/10.1016/j.desal.2020.114445.
[90] Y. Yang, Q. Ding, M. Yang, Y. Wang, N. Liu, X. Zhang, Magnetic ion exchange resin for effective removal of perfluorooctanoate from water: study of a response surface methodology and adsorption performances, Environ. Sci. Pollut. Res. 25 (2018) 29267–29278, https://doi.org/10.1007/s11356-018-2797-1.
[91] T.D. Reynolds, P.A. Richards, Unit Operations and Processes in Environmental Engineering, Second ed., PWS Publishing Company, 1996 (ISBN 978-0534948849).
[92] L. Ding, X. Lu, H. Deng, X. Zhang, Adsorptive removal of 2, 4-dichlorophenoxy-acetic acid (2, 4-D) from aqueous solutions using MIEX resin, Ind. Eng. Chem. Res. 51 (2012) 11226–11235, https://doi.org/10.1021/ie300469h.